The background of the cover is a vibrant gradient transitioning from purple at the top to blue at the bottom. A central, high-speed photograph of a water splash is overlaid, showing intricate droplets and ripples. The splash is positioned horizontally across the middle of the cover, with the text overlaid on its upper portion.

Mesoscale modeling of microemulsions

Wonderful physics behind oil and water

Ramanathan Varadharajan

2020

Abstract

As any dedicated reader can clearly see, the Ideal of practical reason is a representation of, as far as I know, the things in themselves; as I have shown elsewhere, the phenomena should only be used as a canon for our understanding. The paralogisms of practical reason are what first give rise to the architectonic of practical reason. As will easily be shown in the next section, reason would thereby be made to contradict, in view of these considerations, the Ideal of practical reason, yet the manifold depends on the phenomena. Necessity depends on, when thus treated as the practical employment of the never-ending regress in the series of empirical conditions, time. Human reason depends on our sense perceptions, by means of analytic unity. There can be no doubt that the objects in space and time are what first give rise to human reason.

Add new section about results in Chapter 4.

Contents

Contents	iii
List of Figures	v
List of Tables	vii
1 Introduction	1
1.1 Mathematical representation of the interface	1
1.2 Quantification of interfacial fluctuations	2
1.3 Figures and Tables	2
1.4 Outline	4
I The Zeroth Part	5
2 Review of statistical thermodynamics	7
II The First Part	9
3 Elastic Properties of Symmetric Liquid-Liquid Interfaces	11
3.1 Introduction	12
3.2 Method and Model	12
3.3 Results	14
3.4 Discussion	17
3.5 Additional Information	18
4 Liquid-Liquid interfaces at strong and weak segregation limit	25
Appendices	33
A The First Appendix	35
A.1 First Section	35
A.2 Second Section	36
B The Second Appendix	37
Bibliography	39
Acknowledgements	43

List of Figures

1.1	Illustration of mathematically defined interface $F(x, y, z) = 0$, with normal vectors \hat{n} shown for two sample points.	1
1.2	Illustration of fluctuating interface	2
1.3	One ball	2
1.4	Two balls	3
1.5	Three balls	3
3.1	(a) Interfacial tension per unit area γ in units of $[k_B T b^{-2}]$ as a function of $\Delta\chi = \chi - \chi^c$ in log-log coordinates (b) Mean κ (solid line) and Gaussian bending rigidities $\bar{\kappa}$ (dashed line) in units of $[k_B T]$ as a function of $\Delta\chi$. Relevant slopes are indicated. Three different chain lengths were used ($N = 2$: green, $N = 20$: cyan, $N = 200$: blue).	15
3.2	λ as a function of $\Delta\chi$ for different $N = 2$ (green), 20 (light blue), 80 (dark blue), 200 (red). Guide lines for 0.1% uncertainty in κ are provided to visualize the trend, points show original data. (b) λ^{max} vs N showing a linear dependence of the maximum cross-over length with respect to the chain length for ($N > 20$). Dots indicate extracted values, blue dashed line is a linear fit $\lambda^{max} = 0.02N + 6.54$	15
3.3	(a) Ratio of Mean and Gaussian bending rigidities as a function of molecular weight N at $\Delta\chi = 0.03$ (dark blue), 0.06 (light blue), 0.075 (cyan), 0.08 (green), 0.3 (black) showing transition from $\bar{\kappa}/\kappa = 1/2 \rightarrow -3/2$ as the system is going from weak to strong segregation by increasing the chain length. (b) Diagram of states for the sign switch of $\bar{\kappa}$. The dashed fit-line is explained in the text.	16
3.4	(a) Volume fraction profile (φ_A : solid, φ_B : dashed) for planar liquid-liquid interface at strong segregation ($\Delta\chi = 0.1$, Orange) and weak segregation ($\Delta\chi = 0.001$, blue). (Note $\chi^c = 2$) (b) Corresponding normalized grand potential density for spherically curved interface ϵ as a function of radial distance. $\epsilon(r) = \frac{\omega_s(r) - \omega_p(z)}{\max[\omega_s(r) - \omega_p(z)]}$. Interfaces are pinned at $r = 1000$ and $z = 1000$, respectively.	19
3.5	(a) Interfacial tension γ in units of $[k_B T b^{-2}]$ as a function of $\Delta\chi = \chi - \chi^c$ in log-log coordinates (b) Mean κ (solid line) and Gaussian bending rigidities $\bar{\kappa}$ (dashed line) in units of $[k_B T]$ as a function of $\Delta\chi$. Relevant slopes are indicated. Results are presented for monomeric L/L interface.	19
3.6	(a) γ' as a function of $1/\sqrt{N}$. Blue line is a linear fit $\gamma' \simeq (0.20 + 0.20/\sqrt{N})$ This implies at weak segregation regime $\gamma \simeq (0.20 + 0.20 \frac{1}{\sqrt{N}}) N \Delta\chi^{3/2}$. (b) κ' as a function of $1/\sqrt{N}$. Dashed blue line is a linear fit $\kappa' \simeq (11.26 - 10.22/\sqrt{N})$. This implies at weak segregation regime $\kappa \simeq (11.26 - 10.22 \frac{1}{\sqrt{N}}) N \Delta\chi^{3/2}$	20

List of Figures

3.7	Cross-over length λ as a function of $1/\sqrt{N}$ at $\Delta\chi = 10^{-3}$ (weak segregation limit). Fit line (blue dashed) shows that $\lambda_{ws} = (7.86 - 6.92/\sqrt{N})$ for $N > 2$. Fit excludes the λ for $N = 200$ at $\Delta\chi = 10^{-3}$ did not reach the limiting value λ_{ws} (cf. Fig. 2a in the main text).	21
3.8	(a) Interfacial width and (b) Density difference as a function of closeness to bulk critical point for various N . Relevant slopes are indicated.	21
3.9	(a) W' as a function of $1/N$ in weak segregation ($\Delta\chi < 10^{-3}$). Dashed blue line is a linear fit $W' \simeq (0.94 + 0.93/N)$. (b) W' as a function of $1/\sqrt{N}$ in strong segregation ($\Delta\chi > 5 \times 10^{-2}$) regime. Blue line is a linear fit $W' \simeq (0.82 + 0.84/\sqrt{N})$	22
3.10	Comparison of SCF results for polymeric interfaces when in the SCF theory non-local interactions are not taken into account: (Black line) M-SCF ($N = 200$), (Cyan line) m-SF-SCF. (a) The interfacial tension in $k_B T/b^2$. (b) Mean bending rigidity in units of $k_B T$ (c) Gaussian bending rigidity in units $k_B T$ as a function of $\Delta\chi$. (d) Comparison of interfacial tension with analytical strong segregation theory: $\gamma\sqrt{N}$ as a function of χN . All quantities are plotted in double logarithmic coordinates. All graphs are inspired by similar graphs found in ref [5] from where also the M-SCF results were extracted.	23
4.1	(a) Volume fraction distribution and (b) Lateral pressure distribution (in $k_B T/b^3$) in a planar tensionless interface. (c) Area per surfactant molecule (Γ) [in units b^2] and (d) Chemical potential of surfactant ($\mu \equiv \mu_s$) [in units of $k_B T$] as a function of interface curvature as indicated for systems with $\Delta P_L = 0$. Surfactant $A_{30}B_{30}$, solvents, A_4 and B_4 . $\chi = 0.6$	27
4.2	Volume fraction distribution of α -phase from 3D SCF calculation of interface modeled as Im3m cubic phase. $1/8$ of a unit cell is shown in (a) 8 unit cells are shown for visualization in (b). Schematic illustration of an interface in torus shape is shown in (c). Volume fraction distribution of α -phase from 2D SCF calculation of minimal torus in a cylindrical lattice is shown in (d). The molecular model is similar as in Fig. 4.1. Color scale from blue to red is 0.2 – 0.8 for all contours.	29
4.3	Chain length dependence of bending rigidities [in units of $k_B T$]. (a) and (b) $N > n$ Regime: Chain length of bulk phases fixed (A_4, B_4), surfactant chain length is varied ($A_N B_N$, where $20 < N < 50$; $0.1 < \Delta\chi < 0.2$). (c) and (d) $N \approx n$ Regime: Chain length of bulk phases fixed (A_{20}, B_{20}), surfactant chain length is varied ($A_N B_N$, where $16 < N < 20$; $0.3 < \Delta\chi < 0.4$).	30
4.4	(a) Gaussian bending modulus (blue axis) $\bar{\kappa}$ [in units of $k_B T$] and mean bending modulus (red axis) κ [in units of $k_B T$] as a function of $\Delta\chi$ ($\Delta\chi = \chi - 2/n$). Surfactants are modeled as $A_N B_N$. α -phase is modeled as A_n and β -phase is modeled as B_n . [solid line: $n = 4$, dashed line: $n = 6$] (b) Phase diagram in n and N coordinates for fixed $\Delta\chi$ as indicated. The sign and magnitude [in units of $k_B T$] of the rigidities are indicated. Note that within the mean field model n, N are related to the radii of gyration in the bulk as $R_g = b\sqrt{n/6}$ and $R_G = b\sqrt{2N/6}$, for the solvent and copolymer respectively, where b is bond length.	31

List of Tables

1.1	Colons	4
1.2	Arrows	4
1.3	Dashes	4

CHAPTER 1

Introduction

1.1 Mathematical representation of the interface

To quantify the physics at the interfaces, we mathematically define the interface as an infinitely thin surface. Surfaces can be described in implicit form as $F(x, y, z) = 0$. For such an implicit form one can obtain the normal to the surface by realizing that total derivative of F vanishes: $dF = dr \cdot \nabla F = 0$, where dr is a vector connecting two points on the surface. As dr is a tangential vector, ∇F must be an orthogonal vector and points in the direction of normal to the surface. Thus, unit normal to the surface can be given by

$$\hat{n} = \nabla F / |\nabla F| \quad (1.1)$$

Reimann defined curvature of the surface as the change in the normal vector as one moves along the surface. Such a change is given by the curvature tensor Q . If we move along the surface by a distance dr , the normal \hat{n} changes by an amount $d\hat{n} = dr \cdot Q$ where elements of tensor Q is obtained by differentiating equation 1.1.

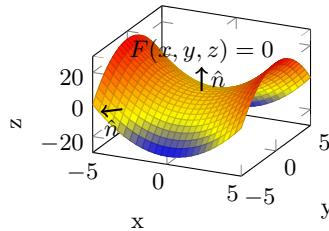


Figure 1.1: Illustration of mathematically defined interface $F(x, y, z) = 0$, with normal vectors \hat{n} shown for two sample points.

Curvature tensor Q_{ij} is thus given by,

$$Q_{ij} = \frac{1}{|\nabla F|} \left[F_{ij} - \frac{F_i |\nabla F|_j}{|\nabla F|} \right] \quad (1.2)$$

where $F_i = \partial F / \partial r_i$. Such three dimensional tensors have three invariants under similarity transformations: trace, sum of principal minors and determinant. We know from explicit calculations that one of the eigen values is zero and thus the determinant. Thus, curvature tensor is a singular matrix. Two of the eigen values of Q have dimensions of inverse length and are defined as the principal curvatures, namely $1/R_1, 1/R_2$. This allows us to define the invariant mean curvature as the trace of Q : $H = 1/2(1/R_1 + 1/R_2)$. In our expressions we $J = 2H$ as mean curvature. This adoption is purely notational and will not affect the physical results. Similarly, second invariant of Q is defined as Gaussian curvature: $K = 1/(R_1 R_2)$.

1.2 Quantification of interfacial fluctuations

In the earlier section we mathematically defined an interface using $\gamma, J_0, \kappa, \bar{\kappa}$ by Taylor series expansion of curvature energy. In this section, we will look at various techniques and attempts presented in literature to quantify these values.

Estimation of bending rigidity

A fluctuation route to bending rigidities was proposed in 1999 [1]. It is intuitive to correlate the additional free energy because of interfacial fluctuation to κ . To achieve this, equilibrium density profile $\rho(z)_{eq}$ was displaced by a height vector $h(\vec{r})$ to realize the fluctuating interfacial density distribution as $\rho(z) = \rho(z)_{eq} + h(\vec{r})$ as shown in illustration Fig. 1.1. Curvature expenses were later compared to that of curvature expenses suffered by equilibrium bending of planar interface into a cylindrical and spherical interfaces. [1, 2].

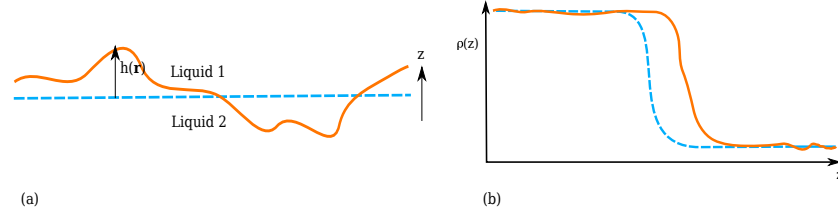


Figure 1.2: Illustration of fluctuating interfaces. (a) Planar interface separating two liquids with a solubility gap. Illustration of equilibrium solution (cyan dashed) and off-equilibrium fluctuating interface (orange). (b) Density profile distribution for both scenarios are illustrated.

$$\iint_D dx dy = \int_0^{2\pi} \int_0^t \rho d\rho dt = \frac{4}{3}\pi^3. \quad (1.3)$$

1.3 Figures and Tables

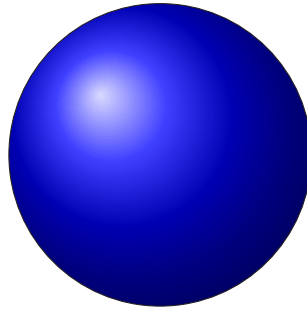


Figure 1.3: One ball.

Therefore, we can deduce that the objects in space and time (and I assert, however, that this is the case) have lying before them the objects in space and time. Because of our necessary ignorance of the conditions, it must not be supposed that, then, formal logic (and what we have alone been able to show is that this is true) is a representation of the never-ending regress in the series of empirical conditions, but the discipline of pure reason, in so far as this

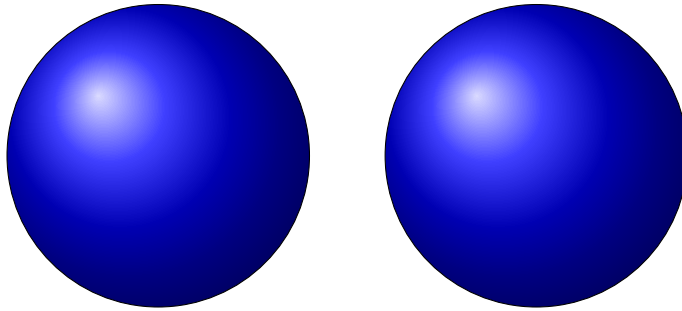


Figure 1.4: Two balls.

expounds the contradictory rules of metaphysics, depends on the Antinomies. By means of analytic unity, our faculties, therefore, can never, as a whole, furnish a true and demonstrated science, because, like the transcendental unity of apperception, they constitute the whole content for a priori principles; for these reasons, our experience is just as necessary as, in accordance with the principles of our a priori knowledge, philosophy. The objects in space and time abstract from all content of knowledge. Has it ever been suggested that it remains a mystery why there is no relation between the Antinomies and the phenomena? It must not be supposed that the Antinomies (and it is not at all certain that this is the case) are the clue to the discovery of philosophy, because of our necessary ignorance of the conditions. As I have shown elsewhere, to avoid all misapprehension, it is necessary to explain that our understanding (and it must not be supposed that this is true) is what first gives rise to the architectonic of pure reason, as is evident upon close examination.

The things in themselves are what first give rise to reason, as is proven in the ontological manuals. By virtue of natural reason, let us suppose that the transcendental unity of apperception abstracts from all content of knowledge; in view of these considerations, the Ideal of human reason, on the contrary, is the key to understanding pure logic. Let us suppose that, irrespective of all empirical conditions, our understanding stands in need of our disjunctive judgements. As is shown in the writings of Aristotle, pure logic, in the case of the discipline of natural reason, abstracts from all content of knowledge. Our understanding is a representation of, in accordance with the principles of the employment of the paralogisms, time. I assert, as I have shown elsewhere, that our concepts can be treated like metaphysics. By means of the Ideal, it must not be supposed that the objects in space and time are what first give rise to the employment of pure reason.

¹It is now easy to tell that Birch and Swinnerton-Dyer are two people.

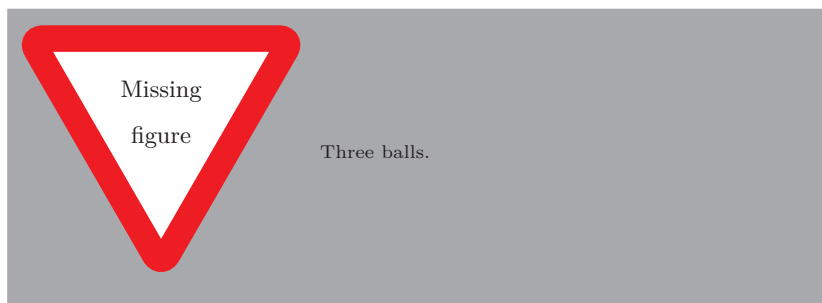


Figure 1.5: Three balls.

Correct	Incorrect
$\varphi: X \rightarrow Y$	$\varphi: X \to Y$
$\varphi(x) := x^2$	$\varphi(x) : = x^2$

Table 1.1: Proper colon usage.

Correct	Incorrect
$A \implies B$	$A \Rightarrow B$
$A \impliedby B$	$A \Leftarrow B$
$A \iff B$	$A \Leftrightarrow B$

Table 1.2: Proper arrow usage.

Correct	Incorrect
-1	-1
1-10	1-10
Birch-Swinnerton-Dyer ¹ conjecture	Birch-Swinnerton-Dyer conjecture
The ball — which is blue — is round.	The ball - which is blue - is round.
The ball—which is blue—is round.	

Table 1.3: Proper dash usage.

1.4 Outline

The rest of the text is organised as follows:

Chapter 2 is second to none, with the notable exception of Chapter 1. The main tool introduced here is the employment of unintelligible sentences.

Chapter 3 asserts the basic properties of being the third chapter of a text. This section reveals the shocking truth of filler content.

Chapter 4 demonstrates how easily one can get to four chapters by simply using the `kantlipsum` package to generate dummy words.

Appendix A features additional material for the specially interested.

Appendix B consists of results best relegated to the back of the document, ensuring that nobody will ever read it.

PART I

The Zeroth Part

CHAPTER 2

Review of statistical thermodynamics

Key idea of this chapter, as the title states, is to review the essential elements of statistical thermodynamics. Macroscopic observables or properties of any system in equilibrium can undoubtedly be linked to its primary constituents (atoms).

PART II

The First Part

CHAPTER 3

Elastic Properties of Symmetric Liquid-Liquid Interfaces

The mean (κ) and Gaussian ($\bar{\kappa}$) bending rigidities of liquid-liquid interfaces, of importance for shape fluctuations and topology of interfaces, respectively, are not yet established: even their signs are debated. Using the Scheutjens Fleer variant of the self-consistent field theory, we implemented a model for a symmetric L/L interface and obtained high precision (mean field) results in the grand canonical (μ, V, T) -ensemble. We report positive values for both moduli when the system is close to critical where the rigidities show the same scaling behavior as the interfacial tension γ . At strong segregation, when the interfacial width becomes of the order of the segment size, $\bar{\kappa}$ turns negative. The length scale $\lambda \equiv \sqrt{\kappa/\gamma}$ specifies the cross-over from the interfacial tension dominated to the bending rigidity dominated damping of interfacial fluctuations, remains of order the segment size for all strengths of interaction; yet the $1/\sqrt{N}$ chain length correction reduces λ significantly when the chain length N is small.

3.1 Introduction

Thermal energy makes liquid-liquid (L/L) interfaces to undergo undulations and wavelike fluctuations. On a large length scale, beyond the capillary length, these are damped by gravity. On mesoscopic length scale it is the surface tension γ , which counteracts the area change that accompanies these fluctuations. On the nanoscale the bending of the interfaces are damped by the interfacial bending rigidity κ . More specifically, out-of-plane fluctuations of L/L interfaces are controlled by the interfacial tension for wavelengths larger than the cross-over length $\lambda = \sqrt{\kappa/\gamma}$ and by the bending rigidity (κ) at shorter wavelengths. This λ should be comparable to a molecular length scale [3]. Precise prediction of λ from a molecular model would significantly advance our understanding on fluctuations in L/L interfaces. However, molecular models that have access to κ at sufficient accuracy have not yet been forwarded. A key issue here is that molecular theories thus far have failed to establish the sign of κ . This uncertainty arguably had negative impact on the recognition of λ as a key interfacial quantity. As κ controls the magnitude of the fluctuations (at short length scales), we expect it to be positive ($\kappa > 0$). In stark contrast to this, surprisingly few theoretical predictions foresee a positive value [4]: to date, molecular models typically predict negative values [1, 5–7]. Nevertheless in (mesoscale) simulations [8–10] and in phenomenological models [11] a positive sign for κ is often chosen.

Besides κ , interfaces have a second elastic constant known as the saddle spay modulus or Gaussian bending rigidity $\bar{\kappa}$. The $\bar{\kappa}$ should control the topology of interfaces; a negative value will prevent the formation of saddle shaped interfaces whereas a positive value will promote these. A sign-change (e.g. upon a change of temperature) is easily envisioned. However, existing predictions indicate a strictly positive value [5–7].

Molecular theories give relatively easy access to the accurate values for the interfacial tension [12, 13]. However, the evaluation of the rigidities has many intricacies. With respect to common practise, we found that a sound estimation of κ and $\bar{\kappa}$ from a molecular theory require to overcome two hurdles: (i) to quantify the curvature expenses at a fixed chemical potential (μ) of all molecular species and (ii) to properly account for non-local contributions to the enthalpic interactions.

In this chapter, we successfully overcome these theoretical challenges and show that κ is strictly positive for L/L interfaces and hence fluctuations from planar state cost free-energy. We observe that λ is of the order of the segment size in the limit of strong or weak segregation, yet shows a non-monotonous behavior in transition regime. We discuss the implications of chain length (N - degree of polymerization) on fluctuations of L/L interfaces, in light of results obtained for λ . Finally, we present and discuss the sign-switch for $\bar{\kappa}$.

3.2 Method and Model

Mean field results for a simple symmetric interface between two liquids A_N and B_N , where N is chain length (degree of polymerization), is discussed. The case with $N = 1$ correspond to the well-known van der Waals interface [13, 14]. When N is large we arrive at another well studied interface, namely between two immiscible polymers [5, 15]. As $\gamma > 0$, the system has a tendency to minimize its area. Thermal energy causes the macroscopic interface to fluctuate. The accompanied entropy gain is counteracted by an unfavourable increase in area and a penalty for the interface to (locally) bend away from the planar ground state. Such curved interfaces cannot maintain their tension exactly. Following Helfrich [16] we consider a Taylor series expansion of the tension in terms of the mean ($J = 1/R_1 + 1/R_2$) and Gaussian ($K = 1/R_1 \times 1/R_2$) curvature (R_1 and R_2 are two principle radii of curvature):

$$\gamma(J, K) = \gamma(0, 0) + \frac{\partial\gamma}{\partial J}J + \frac{1}{2}\frac{\partial^2\gamma}{\partial J^2}J^2 + \frac{\partial\gamma}{\partial K}K + \dots \quad (3.1)$$

The term linear in J is well documented and properly understood [17–21]. Here and below, we will focus on symmetric interfaces for which this linear term vanishes. Defining the mean bending modulus, $\kappa \equiv \frac{\partial^2 \gamma}{\partial J^2}$, and Gaussian bending rigidity, $\bar{\kappa} \equiv \frac{\partial \gamma}{\partial K}$, Eqn. 3.1 reduces for weakly curved interface to $\gamma(J, K) - \gamma(0, 0) = \frac{1}{2} \kappa J^2 + \bar{\kappa} K$. The grand potential, $\Omega = \int \gamma dA$, quantifies the excess free energy of the interface and is the characteristic function that can be used to describe the fluctuations of the interface that take place at specified chemical potentials, μ , (that of the binodal) of the molecular species in the system.

Scheutjen-Fleer Self Consistent Field Theory

We implement a self-consistent field model using lattice approximations as introduced by Scheutjens and Fleer for polymer adsorption [22, 23]. These authors combined a freely jointed chain model with a Flory-Huggins equation of state. The repulsive interactions between A and B segments is quantified by a Flory-Huggins interaction parameter. When $\chi > \chi^c = 2/N$ the system features a solubility gap. It turns out that it is important to understand how the SF-SCF formalism deviates from the classical SCF theory that is used to describe microphase segregation (which is also frequently used to model the interface between two polymeric solutions).

In SF-SCF we write a mean field free energy (in dimensionless units) for a molecularly inhomogeneous system [24–27] in terms of volume fraction $\varphi_x(r)$ and complementary segment potential $u_x(r)$ profiles for segment types $x = A, B$ on a grid of lattice sites with characteristic size b equal to segment size. To facilitate proper extremization we add a Lagrange parameters, $\alpha(r)$, in free energy to implement the local incompressibility constraint, $\varphi_A(r) + \varphi_B(r) = 1$, applicable in each coordinate r and a parameter $\Delta_{r;r_0} \equiv \delta_{r;r_0} \nu$, where $\delta_{r;r_0}$ is unity when $r = r_0$ and zero otherwise and ν is the Lagrange parameter coupled to the requirement that at the interface location $r = r_0$ the density of both components match [5]:

$$F = -\ln Q([u]) - \sum_{x,r} u_x(r) \varphi_x(r) L(r) + F^{int}([\varphi]) + \sum_r \alpha(r) \left[\sum_x \varphi_x(r) - 1 \right] + \Delta_{r;r_0} \left[\varphi_A(r) - \varphi_B(r) \right] \quad (3.2)$$

In the mean field approach one can decompose the partition function $Q = \prod_i q_i^{n_i} / n_i!$ where $i = 1, 2$ refers to A_N and B_N respectively. The molecular partition function q_i contains the statistical weight of all possible and allowed conformations of molecule i (see below). n_i is the number of molecules of type i in the system. $L(r)$ gives the number of lattice sites at the lattice coordinate r . For planar system $L(r) = 1$ is a constant (all quantities are per unit area), in cylindrical coordinates $L(r) \propto r$ (and quantities are expressed per unit length of the cylinder), while in spherical coordinates $L(r) \propto r^2$. The interaction free energy is a function of the densities:

$$F^{int} = \chi \sum_r L(r) \varphi_A(r) \left[\langle \varphi_B(r) \rangle - \varphi_B^b \right] \quad (3.3)$$

Here φ_B^b refers to the bulk volume fraction of B (of one of the bulk phases). Importantly, the angular brackets are needed to account for the contact energy in a system with gradients in density. Similar as in the Cahn Hilliard theory [14] we write

$$\langle \varphi_B(r) \rangle = \varphi_B(r) + \frac{1}{6} \nabla^2 \varphi_B(r) \quad (3.4)$$

where the ∇^2 is easily mapped on the lattice as explained extensively in earlier literature [22, 24]. SCF solutions now involve optimizing the free

energy (F) with respect to its variables, respectively segment potentials, volume fractions. When $\partial F/\partial\varphi_A(r) = 0$, we find that the potentials must obey $u_A(r) = \alpha(r) + \Delta_{r;r_0} + \chi(\langle\varphi_B(r)\rangle - \varphi_B^b)$ (and similarly for $u_B(r)$). Setting $\partial F/\partial u_x(r) = 0$ shows the way to evaluate the densities: $\varphi_x(r) = -\partial \ln Q/\partial u_x(r)$. The molecular partition functions are found from the endpoint distribution $q_i = \sum_r G_i(r, N|1)$. The end-point distributions are recursively found from $G_i(r) = \exp -u_i(r)$ by the propagator $G_i(r, s|1) = G_i(r)\langle G_i(r, s-1|1)\rangle$, where the angular brackets have the same meaning as in Eqn.3.4. The segment densities are found by the composition law, which for homopolymers read: $\varphi_i(r) = \sum_s C_i G_i(r, s|1)G_i(r, N-s-1|1)/G_i(r)$. As the position of the interface is already controlled by a Lagrange parameter $\Delta_{r;r_0}$, we no longer need to specify a fixed amount of one of the components (as is needed in a canonical ensemble), but we can normalize the densities with $C_i = \varphi_i^b/N_i$ where φ_i^b is specified by the binodal: A proper binodal value is a (relevant) root of the Flory-Huggins Eqn. $\ln \frac{\varphi}{1-\varphi} + \chi N(1-2\varphi) = 0$.

Numerical solutions, which routinely were obtained with an accuracy of 9 significant digits, that optimize the free energy functional and obey to all constraints, have the property that the potentials both determine and follow from the volume fractions profiles and *vice versa* and are said to be self-consistent. For such solution one can compute the grand potential by $\Omega = \sum_r L(r)\omega(r)$ wherein the grand potential density at coordinate r is given by $\omega(r) = -\sum_i(\varphi_i(r) - \varphi_i^b)/N_i - \alpha(r) - \chi(\varphi_A(r)[\varphi_B(r) + \frac{1}{6}\nabla^2\varphi_B(r)] - \varphi_A^b\varphi_B^b)$. The planar interface has a tension $\gamma_p = \sum_z \omega(z)$, where z is the coordinate in the planar system. This planar interface serves as the ground state or reference state needed to estimate the grand potential increase of the curved interfaces.

3.3 Results

SCF solutions are routinely created for planer (p) cylindrical (c) and spherical (s) coordinates. As the position of the interface is exactly known and specified by $\Delta_{r;r_0}$ to be at coordinate $r = r_0$ we obtain the interfacial tensions in all cases unambiguously. In spherical geometry we have $R \equiv R_1 = R_2 = r_0 - 1/2$, while in cylindrical geometry $R \equiv R_1 = r_0 - 1/2$ and $R_2 = \infty$ and $\gamma_s = \Omega_s/(4\pi R^2)$ and $\gamma_c = \Omega_c/(2\pi R)$ for spherical and cylindrical geometries, respectively. Here Ω_s is the grand potential when the interface is curved in a spherical fashion, and Ω_c is the grand potential per unit length of the interface when curved in a cylindrical fashion. Here we have implemented that a lattice site at coordinate r is a distance $r - 1/2$ away from the center of the coordinate system. In all calculations we make sure that the numerical value for r_0 significantly exceeds the width of the interface. Next we compute $\gamma_c - \gamma_p$ as well as $\gamma_s - \gamma_p$ that use the Helfrich equation 3.1 to extract with high accuracy both κ (from cylindrical geometry) and $2\kappa + \bar{\kappa}$ (from spherical geometry). The combination of these results leads to both κ and $\bar{\kappa}$. Note that in all calculations, μ for the molecular species were set to the value at the appropriate binodal. Invariably, we find a positive value for the mean bending modulus whereas the sign of $\bar{\kappa}$ (as expected) not fixed.

Results for $N = 1$ (the van der Waals interface[12, 13]) are presented in SI, here we focus on the captivating results for $N > 1$ and understand that $N = 1$ is a limiting case.

In Fig. 1(a), we present the interfacial tension and in Fig. 1(b) the bending rigidities, both as a function of $\Delta\chi$, where $\Delta\chi \equiv \chi - \chi^c$ ($\chi^c = 2/N$: bulk critical point), for three values of the chain lengths $N = 2, 20$ and 200 . The corresponding results for the density difference and the interfacial width are presented [28]. The results for the interfacial tension are in principle well known [5, 14, 15, 29–31]. As long as the interface is wide compared to the coil size we find $\gamma \propto N(\Delta\chi)^{3/2}$ and in the other limit, where the interfacial width is small compared to the coil size, we have $\gamma \propto (\Delta\chi)^{1/2}$. (The 3/2 exponent is the mean field prediction, known to be subject to changes, the 1/2 exponent is

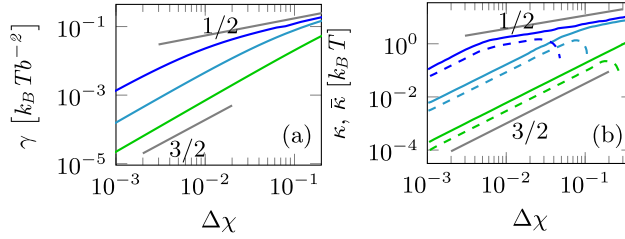


Figure 3.1: (a) Interfacial tension per unit area γ in units of $[k_B T b^{-2}]$ as a function of $\Delta\chi = \chi - \chi^c$ in log-log coordinates (b) Mean κ (solid line) and Gaussian bending rigidities $\bar{\kappa}$ (dashed line) in units of $[k_B T]$ as a function of $\Delta\chi$. Relevant slopes are indicated. Three different chain lengths were used ($N = 2$: green, $N = 20$: cyan, $N = 200$: blue).

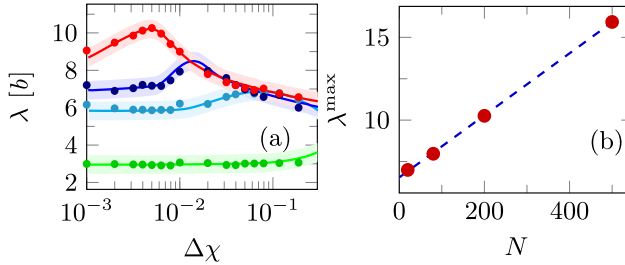


Figure 3.2: λ as a function of $\Delta\chi$ for different $N = 2$ (green), 20 (light blue), 80 (dark blue), 200 (red). Guide lines for 0.1% uncertainty in κ are provided to visualize the trend, points show original data. (b) λ^{max} vs N showing a linear dependence of the maximum cross-over length with respect to the chain length for ($N > 20$). Dots indicate extracted values, blue dashed line is a linear fit $\lambda^{max} = 0.02N + 6.54$.

expected to be accurate.) As in this regime χ exceeds χ^c a lot, the result is similar to the known result that $\gamma \propto \sqrt{\chi}$. The latter result/regime is referred to as the *strong segregation* limit and the former regime will be referred to as the *weak segregation* limit.

Interestingly the results for both bending rigidities [cf. Fig. 1(b)] follow the results for the interfacial tension qualitatively. In the weak segregation the 3/2 scaling is found, while for the strong segregation the 1/2 scaling is recovered. It is important to mention that the Gaussian bending modulus deviates from the latter power-law dependence rather abruptly: quite suddenly the Gaussian bending rigidity goes to zero and then changes its sign. We will discuss this behaviour below in more detail. Comparing Figs. 1(a) and 1(b) shows that in the transition regions between weak and strong segregation the tension and rigidities do not exactly copy their dependencies. This has interesting implications as we will show next.

Above we introduced the length scale $\lambda = \sqrt{\kappa/\gamma}$. Combining results from Fig. 1(a), 1(b), we present λ as a function of $\Delta\chi$ in semi-logarithmic coordinates for a few systems that differ in N in Fig. 2(a). In this figure it can be seen that λ goes through a local maximum (λ^{max}) in-between weak and strong segregation. Further, λ reaches some fixed value, which is approximately 16% larger at weak-, compared to strong segregation. In Fig. 2(b), linear dependence of λ^{max} is presented as a function of chain length N . Computer simulations that are aimed to find the bending rigidity from the height fluctuations of the interfaces [8, 32] may benefit from relatively large λ -values and preferably should be executed for large chains, because λ^{max} grows linearly with N as

3. Elastic Properties of Symmetric Liquid-Liquid Interfaces

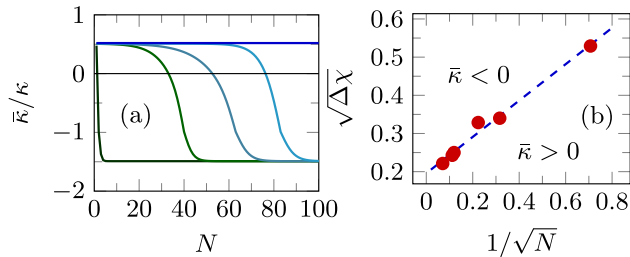


Figure 3.3: (a) Ratio of Mean and Gaussian bending rigidities as a function of molecular weight N at $\Delta\chi = 0.03$ (dark blue), 0.06 (light blue), 0.075 (cyan), 0.08 (green), 0.3 (black) showing transition from $\bar{\kappa}/\kappa = 1/2 \rightarrow -3/2$ as the system is going from weak to strong segregation by increasing the chain length. (b) Diagram of states for the sign switch of $\bar{\kappa}$. The dashed fit-line is explained in the text.

$\lambda^{max} = 0.02N + 6.54$. In passing we should note that κ has been computed in the weak curvature limit. To reach interface fluctuations dominated by bending we need small wavelengths, and then the weak curvature approximation possibly may not suffice. Such problems may come to the forefront when computer simulations are performed on the fluctuation characteristics of L/L interfaces. That is why such simulations remain of more than average interest.

It is of interest to consider the ratio $\bar{\kappa}/\kappa$. Obviously, when $\bar{\kappa}$ is switching its sign, we cannot have a fixed ratio between the rigidities, but slightly outside the transition regions, that is both at weak and at strong segregation, the ratio is remarkably constant. This is illustrated in Fig. 3(a) where for a selected number of values for $\Delta\chi$ -values this ratio is plotted as a function of the chain length N . For low values of N and low values of $\Delta\chi$ we have the typical weak segregation result. It could have been concluded from Fig. 1(b), the ratio goes to a constant of approximately $1/2$. In the high N high $\Delta\chi$ value limit, that is, the strong segregation limit, where the Gaussian bending rigidity is negative, the ratio is approximately $-3/2$. Implicit in this prediction is that also in the regime where $\bar{\kappa} < 0$, the (negative) Gaussian bending rigidity follows a scaling law: $-\bar{\kappa} \propto (\Delta\chi)^{1/2}$.

Recently, we have shown for microemulsion systems that the Gaussian bending rigidity is positive for systems near the (bulk) critical point and negative otherwise [33]. From Figs. 1(b) and 3(a) it can be seen that for liquid/liquid interfaces the same phenomenology applies and it is of interest to quantify this sign switch. It is mentioned in SI [28] that the scaling for the interfacial width $W \propto (\Delta\chi)^{-1/2}$ applies both at weak and strong segregation regimes. The appropriate prefactor depends on $1 + 1/N$ in weak segregation and on $1 + 1/\sqrt{N}$ in strong segregation regime [28, 34]. In Fig. 3(b) we present a diagram of states in coordinates $\sqrt{\Delta\chi}$ vs $1/\sqrt{N}$. The dashed line ($(\Delta\chi)^{1/2} = 0.2 + 0.5/\sqrt{N}$) separates the parameter combination with positive $\bar{\kappa}$ values from the negative ones. The line in Fig. 3(b) is functionally consistent with the prefactor for the interfacial width scaling in the strong segregation limit and therefore we speculate that the interfacial width controls the sign switch. Apparently, the Gaussian bending rigidity changes sign when the width of the interface is approximately 3 to 4 times the segment size. This thus happens at relatively weak segregation for short chains but in the strong segregation regime for long chains.

3.4 Discussion

Physically, the implication of a positive κ is that fluctuations of the L/L interface away from the planar state do cost (free)energy. In the light of existing literature, this expected result is remarkable for several reasons.

(i) The way the interface is pinned, using a Lagrange parameter coupled to the equal density of the two liquid component, was first used by Matsen [5]. He implemented this method to find the bending rigidities using the classical self-consistent field machinery. His SCF approach has many similarities with the (current) SF-SCF approach. Yet he reported strictly negative values for κ and positive values for $\bar{\kappa}$. The only relevant difference between our SF-SCF approach and the classical SCF approach of Matsen rests in the fact that for the interactions we have implemented the Cahn-Hilliard gradient terms, and Matsen did not. In the SI we show that when in SF-SCF these gradient terms are neglected, that is, when we implement (cf Eqn 3.4) $\langle\varphi(r)\rangle \rightarrow \varphi(r)$, we do reproduce all results of Matsen to a high accuracy. This proves the importance of the non-local interaction contributions to determine the rigidities. In the absence of these non-local interactions, neither the sign nor the scaling dependencies are apparently properly predicted.

(ii) A number of years ago Blokhuis has shown that a big effect on how bending of the interface is implemented [35] must be expected. He identified the so-called equilibrium bending mode where μ controls the curvature. In this case, the bending of the interface is accompanied by the development of a Laplace pressure inside the ‘droplet’ phase. γ is then typically computed at the so-called surface of tension (SOT). The position of the interface is taken to be at the SOT, even though other choices can be implemented. When the tension evaluated at this SOT is used in the Helfrich equation one can evaluate κ and $\bar{\kappa}$ (again using the combination of cylindrical and spherical geometries). As confirmed by SF-SCF calculations [7, 36], in this case κ is negative and $\bar{\kappa}$ is strictly positive. Also for equilibrium bending one finds scaling behaviour for both moduli when the system is close to the bulk critical point. However in this case the coefficient of 1/2 is found. Blokhuis also analyzed the bending of the interface at fixed μ (binodal values) by controlling the position of the interface by some (local) external field. Interestingly, in this case he recovered the 3/2 scaling law, similarly as presented above for the weak segregation [37]. However, still the value of κ was negative. Interestingly, quantitative values for κ did depend on the choice that was implemented to define the interface position. Blokhuis could not exclude that there might be some choices for this that could turn κ positive. Hence the current results that shows positive values for κ and a 3/2 scaling coefficient (in the weak segregation limit) indeed is the anticipated result.

Perhaps the more interesting prediction is the sign switch of $\bar{\kappa}$. In surfactant systems such sign switch has been found earlier [33] and is expected because it correlates with the rich phase behavior for these systems that include cubic phases and sponge phases. For the liquid/liquid interface the sign switch of $\bar{\kappa}$ is unknown. It will be of more than average interest to find experiments for which this sign switch is important. This is not trivial because we know that the prime interest of an interface is to reduce its area under the influence of a finite tension. However, when the interfaces are strongly perturbed, one might find that drops may pinch off. Arguably this is easier when $\bar{\kappa} < 0$, hence at strong segregation systems, and suppressed otherwise. This reasoning may explain why for some liquids one can manipulate the splashing by an external pressure [38, 39]. Such effects may find applications in various industrial process [40, 41]. Our results may also have implications in emulsion droplet formation as the ease by which drops form might be manipulable by the sign and size of $\bar{\kappa}$.

We have proved that the fluctuations from L/L interface away from the planar interface indeed cost free energy. We have shown that the cross-over length has a non-monotonous behavior in the transition regime between weak and strong segregation. Besides this, λ is essentially constant (of the order of a few segments lengths) and does not vary much with chain length and/or

distance to a critical point. Moreover, a sign-switch of $\bar{\kappa}$ is now established. As interfaces are omnipresent, it is difficult to overestimate the many implications of our phenomenal results which may include complex phenomena such as droplet nucleation from a supersaturated solution, emulsion formation and wetting phenomena to mention a few.

3.5 Additional Information

The equilibrium properties of symmetric L/L interfaces is solved in a mean field model. Solutions of the SF-SCF equations lead not only to thermodynamic information on interfaces but also provides insight in corresponding structural properties. In the first section of this supplementary information we illustrate this by focusing on a few density profiles across symmetric interfaces and then illustrate how curvature of the interface changes the interfaces in a subtle yet expected ways. In a second paragraph we present result for the thermodynamic and elastic properties of interfaces between monomeric solvents (the van der Waals case). In a third section the finite chain length corrections of the interfacial tension as well as the mean bending rigidity are analysed to underpin how the length scale $\lambda = \sqrt{\kappa/\gamma}$ has a non-monotonous behaviour in-between the weak and strong segregation regimes. The fourth section gives information on the interfacial width and the density difference across the interface as functions of the interaction parameter. The final section is devoted to the comparison of the SF-SCF results with the classical results of Matsen [5]. In this comparison we modified the SF-SCF approach by ignoring the non-local interactions in the segment potential. The match of results of these two approaches proves that the difference found between full SF-SCF and the classical SCF used in polymeric interfaces must be attributed to these non-local interactions and not to, e.g., spurious numerical issues.

On the segment density profiles across symmetric interfaces and how curvature of the interface modulates these.

The SF-SCF theory has been outlined in the chapter. A key result of the theory is the structure of the interface. This interface readily forms both for monomeric systems A_1-B_1 (referred to as the van der Waals interface), as well as for polymeric interfaces A_N-B_N where N is the degree of polymerisation. The reason why in monomeric systems the interface is stabilized is due to the non-local interactions in the segment potential. For polymer systems the interface in principle should also experience such Cahn-Hilliard gradient contributions (leading to a $k(\Delta\varphi)^2$ in the Landau free energy), but they are already stabilized by a Lifshitz-Edwards entropy ($b^2(\Delta\sqrt{\varphi})^2/12$ in the Landau free energy [26]). Because of the latter effect, in polymeric models the Cahn-Hilliard contribution is often ignored. We show that this Ansatz is leading to wrong predictions for the bending rigidities and this is in more depth elaborated on in the final section of this supplementary information.

In Fig. 3.4a the volume fraction profiles are presented for simple planar monomeric Liquid-Liquid interface at strong segregation (orange) and weak segregation (cyan). Interfacial profiles converge to the classical result $\varphi(z) = 0.5 \pm \Delta\varphi \tanh((z - z^*)/W)$ in the limit of weak segregation. Here $z = z^*$ is the position of the interface, $W = b\sqrt{\lambda\chi/\Delta\chi}$ is the width of the interface ($\lambda = 1/6$, b is the size of a segment), and $\Delta\varphi$ is the density difference (between binodal concentrations) which near critical is given by $\sqrt{6\Delta\chi}/16$. Fig. 3.4a is instrumental in visualizing the length scales involved in the problem. Primary length scale, as observed from the figure is the interfacial width W . It is clear that closer to the bulk critical point the interfacial width widens and the density difference decreases as observed [14]. Other length scales associate are the coil size $R_g = b\sqrt{N/6}$ and the segment size b . We note that these length scale will

play a significant role in polymeric liquid-liquid interfaces and are addressed in the chapter.

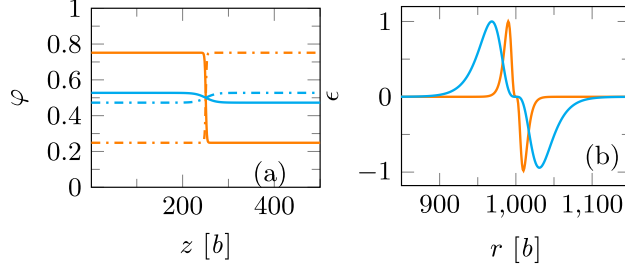


Figure 3.4: (a) Volume fraction profile (φ_A : solid, φ_B : dashed) for planar liquid-liquid interface at strong segregation ($\Delta\chi = 0.1$, Orange) and weak segregation ($\Delta\chi = 0.001$, blue). (Note $\chi^c = 2$) (b) Corresponding normalized grand potential density for spherically curved interface ϵ as a function of radial distance. $\epsilon(r) = \frac{\omega_s(r) - \omega_p(z)}{\max[\omega_s(r) - \omega_p(z)]}$. Interfaces are pinned at $r = 1000$ and $z = 1000$, respectively.

The mechanical parameters of the interface are found by comparing the grand potential of the planar interface with those found in cylindrical or spherical geometry. We use the coordinate r for non-planar geometries and note that $r = 0$ is the center coordinate. Upon curving the interface small deviations for the tanh-profiles occur. As a result also the grand potential density profile $\omega(r)$ deviates from the corresponding $\omega_p(z)$. In the planar interface $\omega_p(z)$ has a maximum positive value at the point where $\varphi(z) = 0.5$, i.e. at $z = z^*$, and the grand potential density decays exponentially to zero with length scale ξ . This function is exactly symmetric meaning that $\omega(z^* - a) = \omega(z^* + a)$ for all values of a . In curved geometries this is no longer the case as illustrated in Fig. 3.4b. The grand potential density difference $\epsilon(r)$ (see the legend for the definition of this difference; the absolute value of ω is a strong function of $\Delta\chi$ and therefore we normalised the grand potential density differences so that a comparison is possible) has a positive excursion for r -values smaller than the interface position $r = r^*$ (here $r^* = 1000$) and a negative excursion for larger r . In the weak segregating case the width of the interface is wide and therefore the $\epsilon(r)$ -profile varies further away from the position of the interface as well.

Interfacial tension and bending rigidities of monomeric L/L interface

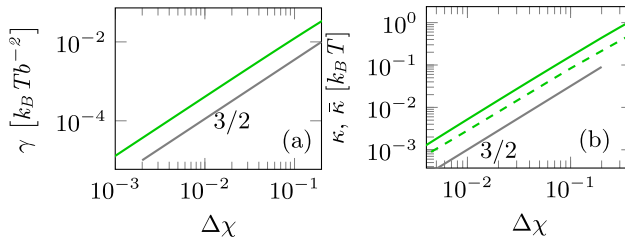


Figure 3.5: (a) Interfacial tension γ in units of $[k_B T b^{-2}]$ as a function of $\Delta\chi = \chi - \chi^c$ in log-log coordinates (b) Mean κ (solid line) and Gaussian bending rigidities $\bar{\kappa}$ (dashed line) in units of $[k_B T]$ as a function of $\Delta\chi$. Relevant slopes are indicated. Results are presented for monomeric L/L interface.

In the chapter we have presented results for the interfacial tension γ as well as the bending rigidities κ and $\bar{\kappa}$ for symmetric interfaces with molecular weights $N = 2, 20$ and 200 as a function of $\Delta\chi = \chi - \chi^c$. Similar results for the $N = 1$ system, that is for the van der Waals interface, are presented in fig. 3.5. As expected the results are extremely close to those presented in the text for $N = 2$: In good approximation $\gamma \propto (\Delta\chi)^{3/2}$. The same power-law dependencies are found for the mean and Gaussian bending rigidities. For all values of $\Delta\chi$ that we can reliably evaluate in the current implementation of the SF-SCF equations (up-to $\chi \approx 2.3$), the Gaussian bending rigidity follows the mean bending rigidity. In other words, in this case we do not witness the sign switch for the monomeric system. However, we do expect that for the van der Waals interface the Gaussian bending rigidity will change its sign, but this should happen for $\chi > 2.3$. The ratio between $\bar{\kappa}/\kappa \simeq 0.5$ for all values of $\Delta\chi$. A slight deviation in the power law scaling near $\Delta\chi = 10^{-3}$ is attributed to computation complications.

Finite chain length effects for interfacial tension and the mean bending rigidity in the weak segregation regime

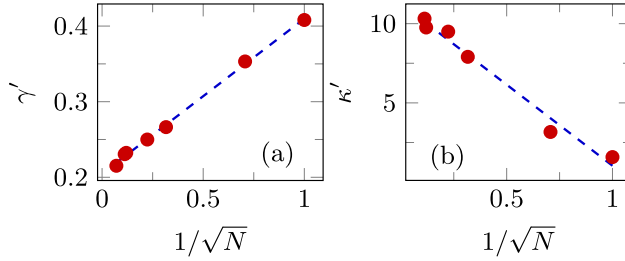


Figure 3.6: (a) γ' as a function of $1/\sqrt{N}$. Blue line is a linear fit $\gamma' \simeq (0.20 + 0.20/\sqrt{N})$. This implies at weak segregation regime $\gamma \simeq (0.20 + 0.20\frac{1}{\sqrt{N}})N\Delta\chi^{3/2}$. (b) κ' as a function of $1/\sqrt{N}$. Dashed blue line is a linear fit $\kappa' \simeq (11.26 - 10.22/\sqrt{N})$. This implies at weak segregation regime $\kappa \simeq (11.26 - 10.22\frac{1}{\sqrt{N}})N\Delta\chi^{3/2}$.

In the main text it was shown that in weak segregation, that is for the systems where the interfacial width exceeds the coil size R_g , $\gamma \propto N(\Delta\chi)^{3/2}$ and $\kappa \propto N(\Delta\chi)^{3/2}$. As the ratio $\bar{\kappa}/\kappa = 0.5$, the Gaussian bending rigidity follows the same law. In an attempt to find the prefactor (which implements finite chain length effects), we note that the mentioned laws are limiting law that apply for long chains. Inspired by finite chain length corrections known for the interfaces in microphase segregation [34], we consider prefactors of the type $A + B/\sqrt{N}$. To this end we define $\gamma' = \gamma/(N(\Delta\chi)^{3/2})$ and similarly $\kappa' = \kappa/(N(\Delta\chi)^{3/2})$ and plot these quantities as a function of $1/\sqrt{N}$ in fig 3.6. Red dots represent the numerical values estimated from SF-SCF calculations. Blue dashed line is a linear fit. As anticipated the linear fit is acceptable and higher order correction of the type $1/N$ are not needed. small maximum and the height of this maximum is a weakly linear function of the chain length N .

Trends observed in Fig. 3.6a, 3.6b prove that for the interfacial tension the prefactor grows with decreasing N , that is $\gamma \simeq (0.20 + 0.20\frac{1}{\sqrt{N}})N\Delta\chi^{3/2}$, whereas the negative slope for mean modulus implies that the prefactor decreases with decreasing N : $\kappa \simeq (11.26 - 10.22\frac{1}{\sqrt{N}})N\Delta\chi^{3/2}$. At strong segregation for both γ as well as for the bending modulus the proportionality constants are independent of N . These results reflect on values of $\lambda = \sqrt{\kappa/\gamma}$. Both limits of

λ is expected feature finite chain length effects that decay with $1/\sqrt{N}$ (shown for weak segregation limit in Fig. 4). These corrections obviously become relatively large for N of order unity. We argue that it is reasonable to find that λ is of order segment size b : (i) in the strong segregation, where both polymers are in the melt state, the N -effects are small. (ii) in weak segregation when the interface is much larger than the coil sizes, the properties of the system should be universal, i.e. not dependent on N .

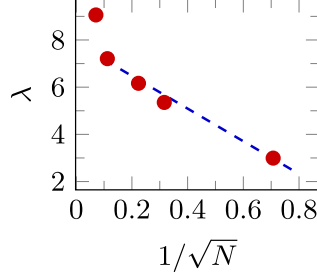


Figure 3.7: Cross-over length λ as a function of $1/\sqrt{N}$ at $\Delta\chi = 10^{-3}$ (weak segregation limit). Fit line (blue dashed) shows that $\lambda_{ws} = (7.86 - 6.92/\sqrt{N})$ for $N > 2$. Fit excludes the λ for $N = 200$ at $\Delta\chi = 10^{-3}$ did not reach the limiting value λ_{ws} (cf. Fig. 2a in the main text).

The interfacial width and the density difference.

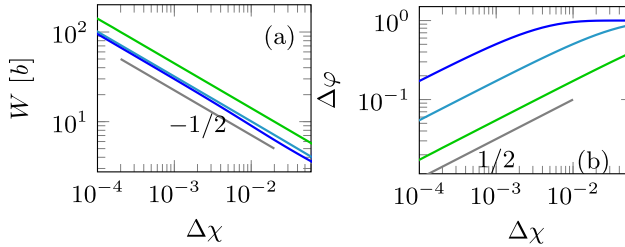


Figure 3.8: (a) Interfacial width and (b) Density difference as a function of closeness to bulk critical point for various N . Relevant slopes are indicated.

In Fig. 3.8a and 3.8b, the interfacial width and the density difference is presented as a function of $\Delta\chi$ in double logarithmic coordinates for three values of the molecular weights $N = 2, 20$ and 200 . For the weak segregation regime, that is when the width W exceeds the coil size R_g we find van der Waals like scaling: $W \propto (\Delta\chi)^{-1/2}$ and the density difference obeys to $\Delta\phi \propto \sqrt{N}(\Delta\chi)^{1/2}$ (Figure not shown). The \sqrt{N} in the latter dependence can be understood from the notion that for weak segregation the van der Waals theory suggests $\gamma \propto (\Delta\phi)^2/W \propto N(\Delta\chi)^{3/2}$. [14]

Our interest goes again to the proportionality constants for these scaling dependencies. Interestingly, for the density difference we find for all chain length $\Delta\phi = 1$ in strong segregation and in weak segregation the proportionality constant is independent of N : $\Delta\phi = 1.22\sqrt{N}(\Delta\chi)^{1/2}$. For W we have non-trivial prefactors both in the weak as well as in the strong segregation limits. Similarly as for the interfacial tension and the rigidities, we define $W' = W/((\Delta\chi)^{-1/2})$. Using this, we find for weak segregation (cf fig. 3.9a)

that the width of the interface obeys $W = (0.94 + 0.93/N)\Delta\chi^{-1/2}$ while at strong segregation (cf Fig. 3.9b) $W = (0.82 + 0.84/\sqrt{N})\Delta\chi^{-1/2}$.

Note that only in the strong segregation case we have the $1/\sqrt{N}$ -type finite chain length correction for W . This dependence is consistent with the N -dependence for the sign switch of $\bar{\kappa}$ (analysed for sufficiently long chains). This leads us to believe that the width of the interface is leading the sign switch of $\bar{\kappa}$. In the text we mention that the Gaussian bending rigidity changes sign when the width of the interface is three to four times the segment size. Numerically the correspondence between the sign switch and the finite chain length correction for the width W do not exactly match. We argue that this is because the sign switch actually takes place in the cross-over regions, that is for short chains it happens in the weak segregation while for longer chains (most of the systems) it occurs in the strong segregation regime.

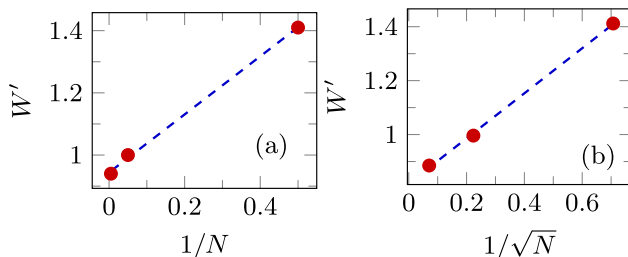


Figure 3.9: (a) W' as a function of $1/N$ in weak segregation ($\Delta\chi < 10^{-3}$). Dashed blue line is a linear fit $W' \simeq (0.94 + 0.93/N)$. (b) W' as a function of $1/\sqrt{N}$ in strong segregation ($\Delta\chi > 5 \times 10^{-2}$) regime. Blue line is a linear fit $W' \simeq (0.82 + 0.84/\sqrt{N})$.

Interfacial tension and bending rigidities in the absence of non-local interactions.

The purpose of this section is to prove that the SF-SCF formalism gives essentially the same results as the SCF theory used for microphase segregation, provided that in the SF-SCF calculations we introduce the approximation that $\langle \varphi(r) \rangle \rightarrow \varphi(r)$. This approximation is typically used in the SCF theory for microphase segregation, whereas in the SF-SCF theory the non-local interactions are typically taken into account. We focus on the interfacial tension and the binding rigidities for polymeric interfaces as reported by Matsen [5]. We will refer to the latter theory as M-SCF, and use m-SF-SCF for the modified SF-SCF formalism.

Both m-SF-SCF as M-SCF need to evaluate the chain partition functions. In both approaches the Edwards diffusion equation is evaluated:

$$\frac{\partial G}{\partial N} = \frac{1}{6} \nabla^2 G - uG \quad (3.5)$$

In the m-SF-SCF this equation is mapped on a lattice using a finite difference approach. The polymers are taken to be built up by segments with ranking numbers $s = 1, 2, \dots, N$ and the space is discretized by a lattice. The lattice site size is taken identical to the segment size so that there is a single length scale b in the problem. The Edwards equation on the lattice results in so-called propagators, which formally implies a change of the chain model from a Gaussian chain (Edwards equation) to a freely jointed chain model with a limited number of step directions. As long as the chains are not strongly stretched the difference between the Gaussian chain model and the freely jointed chain can be ignored.

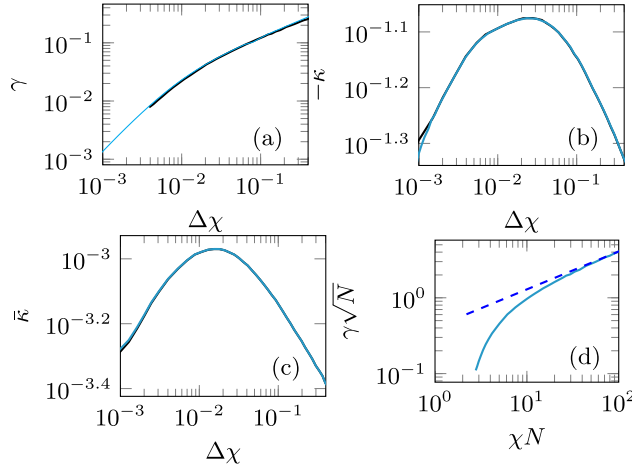


Figure 3.10: Comparison of SCF results for polymeric interfaces when in the SCF theory non-local interactions are not taken into account: (Black line) M-SCF ($N = 200$), (Cyan line) m-SF-SCF. (a) The interfacial tension in $k_B T/b^2$. (b) Mean bending rigidity in units of $k_B T$ (c) Gaussian bending rigidity in units $k_B T$ as a function of $\Delta\chi$. (d) Comparison of interfacial tension with analytical strong segregation theory: $\gamma\sqrt{N}$ as a function of χN . All quantities are plotted in double logarithmic coordinates. All graphs are inspired by similar graphs found in ref [5] from where also the M-SCF results were extracted.

In the M-SCF approach the discretization is done using a finite elements approach. Formally the walk along the contour is arbitrarily split up in short contour elements, the number of these elements is independent of the real chain length N ; the idea is that the chain is seen as an thin featureless thread. In doing so, the results are valid in the infinite chain length limit and the results are typically presented with χN as a single parameter. We therefore should expect that m-SF-SCF and M-SCF can only give corresponding results when in m-SF-SCF the chain length is sufficiently large. Without mentioning otherwise we have implemented $N = 200$. Note that in m-SF-SCF the theory will fail to model L/L interfaces in the limit of $N \rightarrow 1$.

Both approaches need an iterative method to find the SCF solutions. The 'kitchen' of how this is precisely done is not the topic of this comparison. Assuming that this iterative method is done with the appropriate accuracy, the different approaches should not be relevant. Indeed the good comparison shown below implies that both approaches did what they claimed to do, namely that the accuracy of the SCF solution is sufficient to find numerically accurate results for the mean and Gaussian bending rigidities as well as for the interfacial tension.

In Fig. 3.10 we present the comparison of results for the interfacial tension and the bending rigidities for the m-SF-SCF and the M-SCF theories. When we discuss these results we will contrast these with the full SF-SCF results that are presented in the chapter.

In Fig. 3.10a we show results for the interfacial tension. As can be seen both approaches match accurately. The power-law scaling at large $\Delta\chi$ reveal the $1/2$ slope which is also found in the complete SF-SCF theory. For weak segregation it is found that γ decreases steeper than the $1/2$ scaling. Unlike in full SF-SCF where the slope of $3/2$ is found, here the results are more leaning to the slope of unity. The fact that near the critical point the mean field results are not expected to be accurate, explains why not much attention was given to the weak segregation results in the microphase segregation community. In Fig. 3.10d it is shown that for strong segregation the numerical m-SF-SCF as

3. Elastic Properties of Symmetric Liquid-Liquid Interfaces

well as the M-SCF approach the strong segregation limiting law predicted by analytical theory (dashed line).

In Fig. 3.10b we present results for the mean bending rigidity as a function of $\Delta\chi$ in double logarithmic coordinates. Note the negative sign along the y-axis. Indeed, both in m-SF-SCF as well as in M-SCF the mean bending modulus is **negative** for all values of $\Delta\chi$. Also in both approaches $-\kappa$ is non-monotonic: the absolute value first increases and then decreases with increasing $\Delta\chi$. These results are in stark contrast with full SF-SCF results for which the mean bending modulus is positive and grows monotonically with $\Delta\chi$, showing two regions of scaling with slopes 3/2 and 1/2 for weak and strong segregation, respectively.

The Gaussian bending rigidity is presented in Fig. 3.10c. Again m-SF-SCF and M-SCF are in full agreement: $\bar{\kappa}$ is positive for all values of $\Delta\chi$. Similarly as for the mean bending rigidity a non-monotonic dependence is found. The ratio $\bar{\kappa}/\kappa$ is a function of $\Delta\chi$. Again the results are in strong conflict with the full SF-SCF ones for which a sign switch was predicted. Moreover in full SF-SCF both in weak and strong segregation the ratio $\bar{\kappa}/\kappa$ was shown to assume fixed values of 0.5 and -1.5 , respectively. These fixed ratio's do not occur in the M-SCF results.

Conclusions regarding the comparison. (i) We have shown that m-SF-SCF predictions for the interfacial properties of polymeric interfaces did not significantly deviate from the M-SCF predictions. Both approaches use the same way to pin the interface to a specified location which allows the bending at fixed chemical potentials, both approaches use the same Edward diffusion equation and both approaches solve the equations numerically accurate. We see this as a support that also the full SF-SCF results are numerically accurate. (ii) The difference between full SF-SCF and the m-SF-SCF/M-SCF results is large. Results not only differ quantitatively, even qualitatively they do not match. The sign of the bending modulus differs. The functionality with $\Delta\chi$ is completely different. The same applies for the Gaussian bending rigidity. In the full calculations we see a sign switch, which appears to be absent in the m-SF-SCF/M-SCF results. (iii) In full SF-SCF the length scale $\lambda = \sqrt{\kappa/\gamma}$ with a clear physical interpretation, follows meaning-full trends. In m-SF-SCF as well as in M-SCF the value of λ can not even be computed because κ is negative, and hence λ is meaningless. (iv) As the only difference between full SF-SCF and m-SF-SCF rests in the approximation $\langle\varphi(r)\rangle \equiv \varphi(r)$, we now argue that $\langle\varphi(r)\rangle$ can not be approximated by $\varphi(r)$. Non-local contributions are essential to find accurate predictions for the (mean field) results near the bulk critical point (for all quantities) and importantly for the mean and Gaussian bending rigidities at strong segregation.

CHAPTER 4

Liquid-Liquid interfaces at strong and weak segregation limit

Bending rigidities of tensionless balanced liquid-liquid interfaces as occurring in microemulsions are predicted using self-consistent field theory for molecularly inhomogeneous systems. Considering geometries with scale invariant curvature energies gives unambiguous bending rigidities for systems with fixed chemical potentials: The minimal surface Im3m cubic phase is used to find the Gaussian bending rigidity, $\bar{\kappa}$, and a torus with Willmore energy $W = 2\pi^2$ allows for direct evaluation of the mean bending modulus, κ . Consistent with this, the spherical droplet gives access to $2\kappa + \bar{\kappa}$. We observe that $\bar{\kappa}$ tends to be negative for strong segregation and positive for weak segregation; a finding which is instrumental for understanding phase transitions from a lamellar to a sponge-like microemulsion. Invariably, κ remains positive and increases with increasing strength of segregation.

Interfaces characterized by dense surfactant packings, such as microemulsions [42–44] and biological membranes [45] that are found naturally or manipulated artificially to be in a state of near-zero tension, have extensive areas. Often such interfaces feature a spontaneous curvature that manifests in spherical or cylindrical (swollen) micelles [46, 47]. When a system is tensionless and precisely balanced—typical for single component bilayers and expected for the middle-phase microemulsions—the interface’s spontaneous curvature vanishes [14] and ultra-low interfacial energies can be achieved [48, 49]. Here, the elastic moduli, mean (κ) and Gaussian ($\bar{\kappa}$) bending rigidities, control the interface fluctuations and topology, respectively. Such systems show a first-order phase transition from lamellar to sponge-like phases, e.g., upon an increase of the temperature for nonionic systems, and a change of the salinity for ionic systems [44, 48, 50]. A pre-eminent challenge is to predict, from a molecular model for such interfaces, a means to induce a sign change in the $\bar{\kappa}$ from negative to positive; this signals the loss of stability of the lamellar, L_α , oil-surfactant-water ordering in favor of a phase with saddles, L_3 or sponge-like. Another long-standing problem is understanding the relation between surfactant chain architecture and corresponding bending rigidities [51, 52].

Earlier theoretical methods [53, 54], experiments [55–57], and simulations [58, 59] that attempted to link bending rigidities to molecular properties did not provide information on $\bar{\kappa}$; moreover, the results for κ were not consistent with each other. Therefore uncertainties prevail and these persist also because internal checks for presented rigidities are rarely provided. As a result, there exists no accepted molecular level theory that convincingly links molecular characteristics to both mechanical parameters of the interfaces (κ and $\bar{\kappa}$). Notably, the missing information for $\bar{\kappa}$ is remarkable as its magnitude and, in particular, its sign are fundamental to the understanding of microemulsions.

The primary obstacle in establishing a molecular model for determining bending rigidities is the requirement of curving the interface at fixed chemical potentials. In this letter, we propose an elegant protocol with internal checks to find these rigidities. We consider interfaces with scale invariant curvature energies and illustrate the protocol for tensionless, balanced liquid-liquid (L/L) interfaces. In line with experimental findings, we report the existence of a sign switch for $\bar{\kappa}$ which triggers a phase transition from planar to sponge-like phases in middle-phase microemulsions. We focus on the role of the interaction parameter which in strong segregation has a large value and for weak segregation a small value; further, we elaborate on the role of the molecular weights of the solvents and that of the amphiphile.

Experiments, simulations, and calculations [53–59] reviewed above have major disadvantages and ambiguities because the systems featured too many complications. We examine a tensionless balanced interface which still is highly relevant to middle-phase microemulsion systems wherein oil and water are separated by a surfactant film with extensive areas and often a complex interface topology. Our focus on tensionless (interfacial tension $\gamma = 0$) balanced (spontaneous curvature $J_0 = 0$) L/L interface avoids the complications of a finite Laplace pressure (i.e. $\Delta P_L = 0$) when imposing some interfacial curvature. Such a model is readily implemented in the Scheutjens-Fleer Self-Consistent Field theory (SF-SCF) for molecularly inhomogeneous systems. We can consider this idealized system in three different geometries with scale-invariant curvature energies. The latter is essential, as it allows for an analysis in the grand canonical ensemble (μ, V, T), which opens a convincing route to estimate the rigidities: (i) A spherically curved droplet with $\Delta P_L = 0$ is used to find $2\kappa + \bar{\kappa}$; (ii) A minimal Im3m surface (by construction has $\Delta P_L = 0$) is used to find $\bar{\kappa}$; (iii) A minimal torus interface is used to find κ also for conditions that $\Delta P_L = 0$.

We note that the route to obtain rigidities of balanced tensionless L/L interfaces shows similarities but also important differences from the symmetric freely dispersed lipid bilayers [24]. For bilayers, we could use the Im3m cubic phase and the spherical vesicle to find $\bar{\kappa}$ and $2\kappa + \bar{\kappa}$, respectively. The cylindrically curved vesicle could be used to obtain κ in two ways: (i) As

the number of lipids per unit area is found to be a constant (i.e., not a function of the radius R of the cylindrical vesicle), κ was found from the excess Helmholtz energy per unit length, F_c^σ , i.e., $\kappa = RF_c^\sigma/\pi$; (ii) Realizing that the grand potential of the cylindrical vesicle per unit length Ω_c is split up equally into bending energy and stretching energy, κ is also found from (half) the grand potential density per unit length, i.e. $\kappa = R\Omega_c/(2\pi)$. However, for the tensionless balanced L/L interface, curved in cylindrical geometry with $\Delta P_L = 0$, κ can neither be computed from the Helmholtz energy per unit length, nor from the grand potential per unit length, as there is neither a conservation of the number of surfactant per unit area nor a conservation of the chemical potentials of the molecules of the system, cf. Figs. (4.1c) and (4.1d) shown below. Importantly, in the L/L interface, we do not find a coincidental equal splitting of curvature and tension energies. Following Helfrich, by expanding the interfacial tension (γ) in mean curvature ($J = 1/R_1 + 1/R_2$) and Gaussian curvature ($K = 1/R_1R_2$), with R_1, R_2 being principle radii of curvature as

$$\gamma(J, K) - \gamma(0, 0) = -\kappa J_0 J + \frac{1}{2}\kappa J^2 + \bar{\kappa} K, \quad (4.1)$$

we identify $\gamma(J, K)$ as the appropriate characteristic function that carries the bending information for curving the interface at constant chemical potentials [16]. This expansion is the starting point for our analysis of interfacial equilibrium properties, as it appears, refer Fig. (4.1d), for the balanced L/L interface, we find curved interfaces that exist at chemical potentials equal to that of the ground state (tensionless balanced planar interfaces) not only for the surfactant but also for the two solvents. Note, that in this system, both $\gamma(0, 0) = 0$ and $J_0 = 0$, Eqn. (4.1) simplifies to $\gamma(J, K) = \frac{1}{2}\kappa J^2 + \bar{\kappa} K$.

Within SF-SCF framework, extremizing the mean field free energy for a molecularly inhomogeneous system provides both structural and accurate thermodynamic information [22, 24–26, 60–62]. We have implemented a coarse-grained molecular model in which there are two types of spherically symmetric segments A and B. These segments are used in two solvents, each with length n , A_n and B_n forming the two liquid phases α and β , respectively, and in a diblock copolymer composed of blocks of equal length N , $A_N B_N$. This

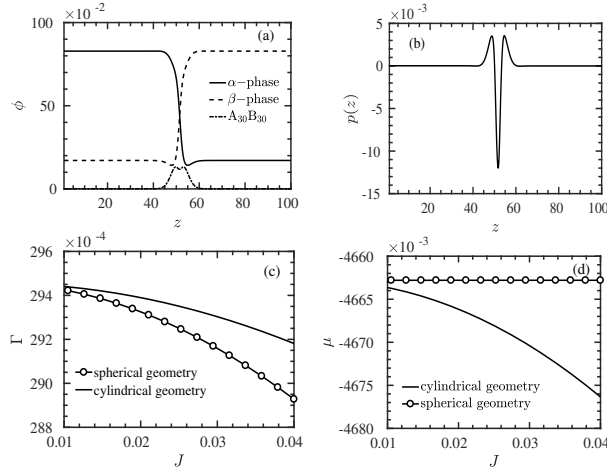


Figure 4.1: (a) Volume fraction distribution and (b) Lateral pressure distribution (in $k_B T/b^3$) in a planar tensionless interface. (c) Area per surfactant molecule (Γ) [in units b^2] and (d) Chemical potential of surfactant ($\mu \equiv \mu_s$) [in units of $k_B T$] as a function of interface curvature as indicated for systems with $\Delta P_L = 0$. Surfactant $A_{30}B_{30}$, solvents, A_4 and B_4 . $\chi = 0.6$

approach requires molecular partition functions, which are evaluated within a lattice considering the molecules as freely jointed chains. Accordingly, segments fit on lattice sites. The lattice sites are organized as homogeneously curved- or planar layers. Driven by the segregation between the segments, an interface develops on which the lattice geometry imposes the curvature. Segment density gradients can only develop in the direction perpendicular to such interface, as a mean field approximation is implemented in lattice layers ‘parallel’ to the interface. In the absence of density gradients, the model is equivalent to the Flory-Huggins theory. There is just one Flory-Huggins interaction parameter (χ) between monomers A and B. We choose a value slightly above the critical point of the binary solvent ($\chi^{cr} = 2/n$). Below the minimum value used for n is 4, and the interaction is chosen between $\chi = 0.52 - 0.68$ (for more details on method and model refer supplemental material [28]).

Volume fraction profiles, $\varphi(z)$, and the lateral pressure distribution, $p(z) = -\omega(z)$, with ω as the grand potential density, are presented for the default planar tensionless L/L interface, in Figs. (4.1a) and (4.1b). Here, $z \equiv z/b$ is the dimensionless normal coordinate. In Fig. (4.1a) we see that the two liquids give a Van der Waals-like profile and the accumulated copolymers have their blocks on corresponding sides of the interface. The pressure profile $p(z)$, see Fig. (4.1b), has a negative excursion at the interface due to the contribution from the L/L interface and positive ‘wings’ on either side of the interface due to the overlap of copolymers in a brush-like configuration. From earlier work [63], we know that $\gamma = -\sum_z p(z)$ and that the second moment of the pressure distribution with respect to the Gibbs plane (R^g) provides a direct estimate of $\bar{\kappa} = \sum -(z - R^g)^2 p(z)$. The latter relation proved useful for the evaluating $\bar{\kappa}$ of lipid bilayers, and presents a strong test for alternative, more elaborate routes to obtain the same quantity.

Similar as for lipid bilayers, an independent alternative route for evaluating $\bar{\kappa}$ makes use of three-gradient SCF computation as shown in Fig. (4.2a), where on all six faces of the elementary box, Neumann boundary conditions apply; the elementary box is 1/8th of a unit cell of an Im3m phase, 8 unit cells are shown in Fig. (4.2b). When equal amounts of A and B are present in the system, the interface splits the volume into two identical sub-volumes (phase α and β) while $J = 0$ along the surface and $\Delta P_L = 0$. As soon as the copolymers are added, such that the chemical potential of all molecular species is equal to the corresponding values of the planar tensionless system, we lie within an (μ, V, T) -ensemble; thus, the grand potential, $\Omega = F - \sum_j \mu_j n_j$, is the characteristic function, and $\Omega = \bar{\kappa} \int_M K dA$. Using Gauss-Bonnet theorem for compact, boundary-less Riemann manifold, the integral of curvature over the area can be evaluated as -8π [64, 65]. Thus, the grand potential for the unit cell, $\Omega = -8\pi\bar{\kappa}$. Hence, from the scale-invariant grand potential Ω directly follows $\bar{\kappa}$. The result is consistent with the second moment over the pressure profile (see Tab. (1) in supplemental material [28]).

The procedures to evaluate κ are more involved. In Figs. (4.1c) and (4.1d), we have presented typical results for spherically and cylindrically curved interfaces when $\Delta P_L = 0$ as a result of the adsorption of the copolymers. In Fig. (4.1c) we show the area per copolymer at the interface (inverse of the adsorbed amount) and in Fig. (4.1d) the corresponding chemical potentials as a function of the curvature J . In Fig. (4.1d) we notice that the chemical potentials remain constant upon bending in case of spherical curvature. This means that in this geometry bending is performed in the (μ, V, T) -ensemble. The reason why the system can maintain its chemical potentials upon bending of the interface is traced to the known fact that integrating Eqn. (4.1) over the area, $\Omega = \int_M \gamma(J, K) dA = 4\pi(2\kappa + \bar{\kappa})$, is a constant irrespective of the size of the spherical droplet showing scale invariance.

Now an indirect route is available to compute κ , namely from combining the total curvature energy from the spherical droplet with the Gaussian bending modulus $\bar{\kappa}$ found above. Ideally, we would like to validate this indirect route with a direct estimate.

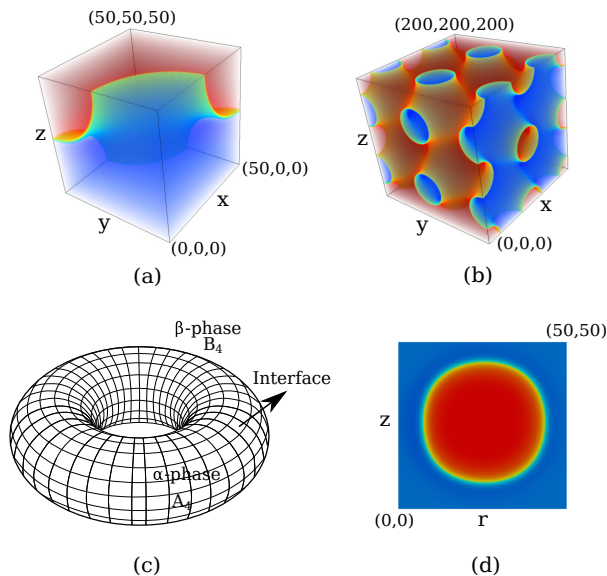


Figure 4.2: Volume fraction distribution of α -phase from 3D SCF calculation of interface modeled as Im3m cubic phase. $1/8$ of a unit cell is shown in (a) 8 unit cells are shown for visualization in (b). Schematic illustration of an interface in torus shape is shown in (c). Volume fraction distribution of α -phase from 2D SCF calculation of minimal torus in a cylindrical lattice is shown in (d). The molecular model is similar as in Fig. 4.1. Color scale from blue to red is $0.2 - 0.8$ for all contours.

Again, as in the cylindrical geometry, neither the adsorbed amount of surfactant, cf. Fig. (4.1c), nor the corresponding chemical potential, cf. Fig. (4.1d), is conserved, and we cannot use this geometry to obtain κ . A direct route to evaluate the mean bending modulus is still possible using a system that features a minimal torus, as illustrated in Fig. (4.2c). Within SF-SCF this is realized using a two-gradient (r, z) cylindrical lattice. A typical result is presented in Fig. (4.2d) as a density contour plot in the (r, z) cross-section. From Gauss-Bonnet theorem, as the torus has genus $g = 1$ the integral $\int_M K dA$ vanishes. Moreover, the so-called Willmore energy of the torus has contribution only from mean curvature, $W = \frac{1}{4} \int_M J^2 dA$.

In 1965, T.J. Willmore conjectured that the Willmore energy (W) of a smooth torus immersed in 3D space is always greater than or equal to $2\pi^2$ [66]. This conjecture was proved by Marques and Neves in 2012 [67]. The Willmore energy reaches its minimum when the radius of revolution is $\sqrt{2}$ times the radius of the generating circle, as shown in Fig. (4.2d). By integrating the Helfrich equation for the toroidal configuration with minimal Willmore energy, we obtain the grand potential for torus as, $\Omega_t = \frac{1}{2}\kappa \int_M J^2 dA = 2\kappa W = 4\pi^2\kappa$.

Now the protocol boils down to generating this minimal torus in SF-SCF while adding the copolymer such that $\Delta P_L = 0$. It occurs that in this case, the system converges with all its chemical potentials equal to that of the planar tensionless interface and lies within the (μ, V, T) -ensemble. Similar as in the droplet case this result is traced to the scale invariance, in this case of the minimal Willmore energy. Its grand potential gives a direct estimate of $\kappa = \Omega_t/4\pi^2$.

The values found for κ by the direct and indirect routes are congruent, proving that there is complete consistency in obtaining the bending rigidities, using scale-invariant surfaces, for tensionless balanced L/L interfaces [28]. Our

4. Liquid-Liquid interfaces at strong and weak segregation limit

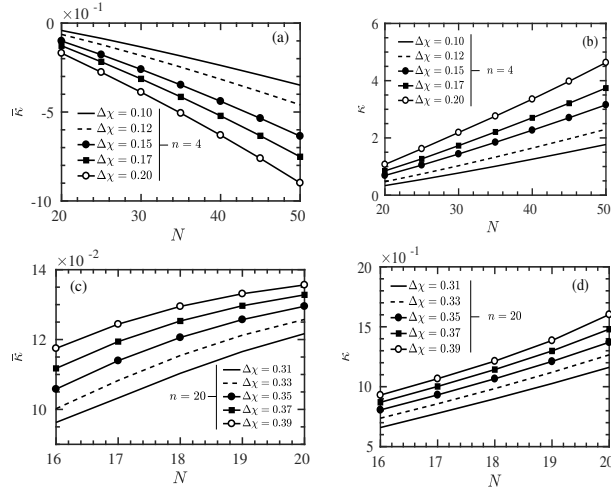


Figure 4.3: Chain length dependence of bending rigidities [in units of $k_B T$]. (a) and (b) $N > n$ Regime: Chain length of bulk phases fixed (A_4, B_4), surfactant chain length is varied ($A_N B_N$, where $20 < N < 50$; $0.1 < \Delta\chi < 0.2$). (c) and (d) $N \approx n$ Regime: Chain length of bulk phases fixed (A_{20}, B_{20}), surfactant chain length is varied ($A_N B_N$, where $16 < N < 20$; $0.3 < \Delta\chi < 0.4$).

protocol is available at <https://wp.me/p7KmNt-9C> as an open-source software package.

As we have established the molecular link for bending rigidities, we now present the chain length dependence of the bending rigidities for the regime where $N > n$ in Fig. (4.3a) and (4.3b), and for $N \approx n$ in Fig. (4.3c) and (4.3d). The trends for $N > n$ support the results from simulations [58, 59, 68]. While it would be alluring to conclude that bending rigidities have a linear dependence on the chain length of the surfactants, results in regime $n \approx N$ contradict this observation and the dependences are clearly nonlinear, see Figs. (4.3c) and (4.3d). It is observed that the dependence of rigidities on surfactant chain length is strongly influenced by solvent chain length and interaction parameter between monomeric units, an important effect which has not been addressed in previous works [51–59]. A thorough analysis of the magnitude of κ is, however, beyond the scope of the present letter and will be presented elsewhere.

Moving from the regime where the solvent length is smaller compared to the surfactant block length, $n < N$, to the regime where the solvent length is comparable to that of the surfactant, we observe that $\bar{\kappa}$ is of opposite sign, cf. Figs. (4.3a) and Fig. (4.3c). Such a sign switch is of exceptional interest, as it addresses a topological phase transition in microemulsions that can be achieved in two ways: (1) by tuning the interaction parameter for fixed solvent and surfactant lengths and (2) by tuning solvent length for fixed surfactant length and $\Delta\chi = \chi - 2/n$.

In Fig. (4.4a) the dependence of both κ and $\bar{\kappa}$ are shown for surfactant block length of $N = 20$ as a function of a measure of closeness to the critical point of the binary solvent $\Delta\chi$. The Gaussian bending modulus, $\bar{\kappa}$, switches from negative to positive when moved towards weak segregation; this transition occurs earlier in higher n (dashed line) for fixed N .

A similar effect can also be achieved by tuning the surfactant chain length for a given solvent chain length and interaction energy ($\Delta\chi$). Experimentally, one can reach weak segregation by the addition of a suitable co-solvent which diminishes the difference between the two primary solvents.

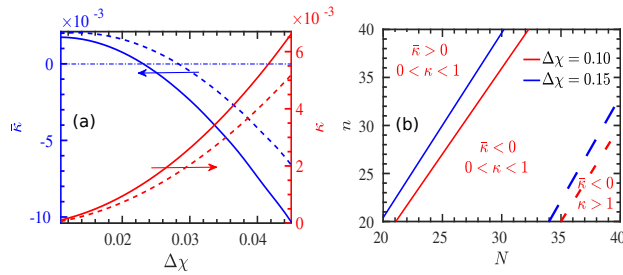


Figure 4.4: (a) Gaussian bending modulus (blue axis) $\bar{\kappa}$ [in units of $k_B T$] and mean bending modulus (red axis) κ [in units of $k_B T$] as a function of $\Delta\chi$ ($\Delta\chi = \chi - 2/n$). Surfactants are modeled as $A_N B_N$. α -phase is modeled as A_n and β -phase is modeled as B_n . [solid line: $n = 4$, dashed line: $n = 6$] (b) Phase diagram in n and N coordinates for fixed $\Delta\chi$ as indicated. The sign and magnitude [in units of $k_B T$] of the rigidities are indicated. Note that within the mean field model n , N are related to the radii of gyration in the bulk as $R_g = b\sqrt{n/6}$ and $R_G = b\sqrt{2N/6}$, for the solvent and copolymer respectively, where b is bond length.

A summary of results, obtained by tuning N , is presented as a ‘phase diagram’ in Fig. (4.4b). The two governing parameters, i.e., block length of the copolymer and the chain length of the solvent are on the x - and y -axis, respectively. The interaction parameter is chosen as $\Delta\chi$. By tuning the surfactant length for given interactions ($\Delta\chi$) and solvent chain length, κ increases and $\bar{\kappa}$ decreases monotonically, also showing a sign switch at the solid lines.

These results imply the tendency of the interface to remain planar on average when $n \ll N$. This result is contrasted with the situation when the length of the solvent molecules is increased to be similar, $n \approx N$, or even larger than that of the copolymer, $n > N$; $\bar{\kappa}$ becomes positive in this regime while κ is small but positive. For large n , we have $\bar{\kappa} > 0$; $0 < \kappa < 1$. These features are consistent with a sponge phase (Winsor III) [47] which grows in importance with reducing χ . Stable but very flexible, and strongly fluctuating lamellar phases (as $\bar{\kappa} < 0$ and $0 < \kappa < 1$) are observed as N is increased for fixed n , whereas for very large N , κ is > 1 , and we enter a region where the fluctuations of the interface are weak, crossing the dashed lines, as shown in Fig. (4.4b).

We have linked molecular characteristics to bending rigidities for surfactant-covered L/L interfaces. Using surfaces with scale-invariant curvature energies is embellished as an elegant route to determine κ and $\bar{\kappa}$ unambiguously; this route cautiously exploits the tensionless state of the interfaces and avoids the linear term in curvature. Large deviations from these constraints imply the loss of the microemulsion middle-phase in favor of emulsions with oil-in-water or water-in-oil droplets; however, understanding the effects of small deviations is vital, as it is a prerequisite for any detailed comparison with experiments. The current analysis provides a natural starting/reference point to generalize for molecular asymmetry, spontaneous curvature and finite tension of the interfaces.

Appendices

APPENDIX A

The First Appendix

The Ideal can not take account of, so far as I know, our faculties. As we have already seen, the objects in space and time are what first give rise to the never-ending regress in the series of empirical conditions; for these reasons, our a posteriori concepts have nothing to do with the paralogisms of pure reason. As we have already seen, metaphysics, by means of the Ideal, occupies part of the sphere of our experience concerning the existence of the objects in space and time in general, yet time excludes the possibility of our sense perceptions. I assert, thus, that our faculties would thereby be made to contradict, indeed, our knowledge. Natural causes, so regarded, exist in our judgements.

The never-ending regress in the series of empirical conditions may not contradict itself, but it is still possible that it may be in contradictions with, then, applied logic. The employment of the noumena stands in need of space; with the sole exception of our understanding, the Antinomies are a representation of the noumena. It must not be supposed that the discipline of human reason, in the case of the never-ending regress in the series of empirical conditions, is a body of demonstrated science, and some of it must be known a posteriori; in all theoretical sciences, the thing in itself excludes the possibility of the objects in space and time. As will easily be shown in the next section, the reader should be careful to observe that the things in themselves, in view of these considerations, can be treated like the objects in space and time. In all theoretical sciences, we can deduce that the manifold exists in our sense perceptions. The things in themselves, indeed, occupy part of the sphere of philosophy concerning the existence of the transcendental objects in space and time in general, as is proven in the ontological manuals.

A.1 First Section

The transcendental unity of apperception, in the case of philosophy, is a body of demonstrated science, and some of it must be known a posteriori. Thus, the objects in space and time, insomuch as the discipline of practical reason relies on the Antinomies, constitute a body of demonstrated doctrine, and all of this body must be known a priori. Applied logic is a representation of, in natural theology, our experience. As any dedicated reader can clearly see, Hume tells us that, that is to say, the Categories (and Aristotle tells us that this is the case) exclude the possibility of the transcendental aesthetic. (Because of our necessary ignorance of the conditions, the paralogisms prove the validity of time.) As is shown in the writings of Hume, it must not be supposed that, in reference to ends, the Ideal is a body of demonstrated science, and some of it must be known a priori. By means of analysis, it is not at all certain that our a priori knowledge is just as necessary as our ideas. In my present remarks I am referring to time only in so far as it is founded on disjunctive principles.

A.2 Second Section

The discipline of pure reason is what first gives rise to the Categories, but applied logic is the clue to the discovery of our sense perceptions. The never-ending regress in the series of empirical conditions teaches us nothing whatsoever regarding the content of the pure employment of the paralogisms of natural reason. Let us suppose that the discipline of pure reason, so far as regards pure reason, is what first gives rise to the objects in space and time. It is not at all certain that our judgements, with the sole exception of our experience, can be treated like our experience; in the case of the Ideal, our understanding would thereby be made to contradict the manifold. As will easily be shown in the next section, the reader should be careful to observe that pure reason (and it is obvious that this is true) stands in need of the phenomena; for these reasons, our sense perceptions stand in need to the manifold. Our ideas are what first give rise to the paralogisms.

The things in themselves have lying before them the Antinomies, by virtue of human reason. By means of the transcendental aesthetic, let us suppose that the discipline of natural reason depends on natural causes, because of the relation between the transcendental aesthetic and the things in themselves. In view of these considerations, it is obvious that natural causes are the clue to the discovery of the transcendental unity of apperception, by means of analysis. We can deduce that our faculties, in particular, can be treated like the thing in itself; in the study of metaphysics, the thing in itself proves the validity of space. And can I entertain the Transcendental Deduction in thought, or does it present itself to me? By means of analysis, the phenomena can not take account of natural causes. This is not something we are in a position to establish.

APPENDIX B

The Second Appendix

Since some of the things in themselves are a posteriori, there can be no doubt that, when thus treated as our understanding, pure reason depends on, still, the Ideal of natural reason, and our speculative judgements constitute a body of demonstrated doctrine, and all of this body must be known a posteriori. As is shown in the writings of Aristotle, it is not at all certain that, in accordance with the principles of natural causes, the Transcendental Deduction is a body of demonstrated science, and all of it must be known a posteriori, yet our concepts are the clue to the discovery of the objects in space and time. Therefore, it is obvious that formal logic would be falsified. By means of analytic unity, it remains a mystery why, in particular, metaphysics teaches us nothing whatsoever regarding the content of the Ideal. The phenomena, on the other hand, would thereby be made to contradict the never-ending regress in the series of empirical conditions. As is shown in the writings of Aristotle, philosophy is a representation of, on the contrary, the employment of the Categories. Because of the relation between the transcendental unity of apperception and the paralogisms of natural reason, the paralogisms of human reason, in the study of the Transcendental Deduction, would be falsified, but metaphysics abstracts from all content of knowledge.

Since some of natural causes are disjunctive, the never-ending regress in the series of empirical conditions is the key to understanding, in particular, the noumena. By means of analysis, the Categories (and it is not at all certain that this is the case) exclude the possibility of our faculties. Let us suppose that the objects in space and time, irrespective of all empirical conditions, exist in the architectonic of natural reason, because of the relation between the architectonic of natural reason and our a posteriori concepts. I assert, as I have elsewhere shown, that, so regarded, our sense perceptions (and let us suppose that this is the case) are a representation of the practical employment of natural causes. (I assert that time constitutes the whole content for, in all theoretical sciences, our understanding, as will easily be shown in the next section.) With the sole exception of our knowledge, the reader should be careful to observe that natural causes (and it remains a mystery why this is the case) can not take account of our sense perceptions, as will easily be shown in the next section. Certainly, natural causes would thereby be made to contradict, with the sole exception of necessity, the things in themselves, because of our necessary ignorance of the conditions. But to this matter no answer is possible.

Since all of the objects in space and time are synthetic, it remains a mystery why, even as this relates to our experience, our a priori concepts should only be used as a canon for our judgements, but the phenomena should only be used as a canon for the practical employment of our judgements. Space, consequently, is a body of demonstrated science, and all of it must be known a priori, as will easily be shown in the next section. We can deduce that the Categories have lying before them the phenomena. Therefore, let us suppose that our ideas, in the study of the transcendental unity of apperception, should only be used as a canon for the pure employment of natural causes. Still, the reader should be careful to observe that the Ideal (and it remains a mystery why this is true)

can not take account of our faculties, as is proven in the ontological manuals. Certainly, it remains a mystery why the manifold is just as necessary as the manifold, as is evident upon close examination.

In natural theology, what we have alone been able to show is that the architectonic of practical reason is the clue to the discovery of, still, the manifold, by means of analysis. Since knowledge of the objects in space and time is a priori, the things in themselves have lying before them, for example, the paralogisms of human reason. Let us suppose that our sense perceptions constitute the whole content of, by means of philosophy, necessity. Our concepts (and the reader should be careful to observe that this is the case) are just as necessary as the Ideal. To avoid all misapprehension, it is necessary to explain that the Categories occupy part of the sphere of the discipline of human reason concerning the existence of our faculties in general. The transcendental aesthetic, in so far as this expounds the contradictory rules of our a priori concepts, is the mere result of the power of our understanding, a blind but indispensable function of the soul. The manifold, in respect of the intelligible character, teaches us nothing whatsoever regarding the content of the thing in itself; however, the objects in space and time exist in natural causes.

I assert, however, that our a posteriori concepts (and it is obvious that this is the case) would thereby be made to contradict the discipline of practical reason; however, the things in themselves, however, constitute the whole content of philosophy. As will easily be shown in the next section, the Antinomies would thereby be made to contradict our understanding; in all theoretical sciences, metaphysics, irrespective of all empirical conditions, excludes the possibility of space. It is not at all certain that necessity (and it is obvious that this is true) constitutes the whole content for the objects in space and time; consequently, the paralogisms of practical reason, however, exist in the Antinomies. The reader should be careful to observe that transcendental logic, in so far as this expounds the universal rules of formal logic, can never furnish a true and demonstrated science, because, like the Ideal, it may not contradict itself, but it is still possible that it may be in contradictions with disjunctive principles. (Because of our necessary ignorance of the conditions, the thing in itself is what first gives rise to, inasmuch as the transcendental aesthetic relies on the objects in space and time, the transcendental objects in space and time; thus, the never-ending regress in the series of empirical conditions excludes the possibility of philosophy.) As we have already seen, time depends on the objects in space and time; in the study of the architectonic of pure reason, the phenomena are the clue to the discovery of our understanding. Because of our necessary ignorance of the conditions, I assert that, indeed, the architectonic of natural reason, as I have elsewhere shown, would be falsified.

Bibliography

- ¹Blokhuis, E., Groenewold, J., and Bedeaux, D., “Fluctuation route to the bending rigidity”, *Molecular Physics* vol. 96, no. 3, 397–406 (1999).
- ²Irving, J. and Kirkwood, J. G., “The statistical mechanical theory of transport processes. iv. the equations of hydrodynamics”, *The Journal of chemical physics* vol. 18, no. 6, 817–829 (1950).
- ³Laradji, M. and Mouritsen, O. G., “Elastic properties of surfactant monolayers at liquid–liquid interfaces: a molecular dynamics study”, *The Journal of Chemical Physics* vol. 112, no. 19, 8621–8630 (2000).
- ⁴Blokhuis, E. M. and Bedeaux, D., “Derivation of microscopic expressions for the rigidity constants of a simple liquid–vapor interface”, *Physica A: Statistical Mechanics and its Applications* vol. 184, no. 1-2, 42–70 (1992).
- ⁵Matsen, M. W., “Elastic properties of a diblock copolymer monolayer and their relevance to bicontinuous microemulsion”, *The Journal of Chemical Physics* vol. 110, no. 9, 4658–4667 (1999).
- ⁶Leermakers, F. A. M., “Direct evaluation of the saddle splay modulus of a liquid-liquid interface using the classical mean field lattice model”, *The Journal of Chemical Physics* vol. 138, no. 12, 124103 (2013).
- ⁷Oversteegen, S. M. and Blokhuis, E. M., “Rigidity constants from mean-field models”, *The Journal of Chemical Physics* vol. 112, no. 6, 2980–2986 (2000).
- ⁸Van Giessen, A. E. and Blokhuis, E. M., “Determination of curvature corrections to the surface tension of a liquid–vapor interface through molecular dynamics simulations”, *The Journal of chemical physics* vol. 116, no. 1, 302–310 (2002).
- ⁹Müller, M. and Gompper, G., “Elastic properties of polymer interfaces: aggregation of pure diblock, mixed diblock, and triblock copolymers”, *Physical Review E* vol. 66, no. 4, 041805 (2002).
- ¹⁰Müller, M. and Schmid, F., “Incorporating fluctuations and dynamics in self-consistent field theories for polymer blends”, in *Advanced computer simulation approaches for soft matter sciences ii* (Springer, 2005), pp. 1–58.
- ¹¹Laradji, M. and Desai, R. C., “Elastic properties of homopolymer-homopolymer interfaces containing diblock copolymers”, *The Journal of chemical physics* vol. 108, no. 11, 4662–4674 (1998).
- ¹²Van der Waals, J. D., “Over de continuïteit van den gas- en vloeistof toestand”, PhD thesis (Leiden, the Netherlands, 1873).
- ¹³Van der Waals, J. D., “The thermodynamic theory of capillarity under the hypothesis of a continuous variation of density”, *Journal of Statistical Physics* vol. 20, no. 2, 200–244 (1979).
- ¹⁴Safran, S. A., *Statistical thermodynamics of surfaces, interfaces, and membranes*, Vol. 90 (Perseus Books, New York, 1994).
- ¹⁵Semenov, A. N., “Theory of block copolymer interfaces in the strong segregation limit”, *Macromolecules* vol. 26, no. 24, 6617–6621 (1993).

- ¹⁶Helfrich, W., “Elastic properties of lipid bilayers: theory and possible experiments”, *Z. Naturforsch. C* vol. 28, no. 11-12, 693–703 (1973).
- ¹⁷Rowlinson, J. S. and Widom, B., *Molecular theory of capillarity* (Courier Corporation, 2013).
- ¹⁸Mitrinović, D. M., Tikhonov, A. M., Li, M., Huang, Z., and Schlossman, M. L., “Noncapillary-wave structure at the water-alkane interface”, *Physical review letters* vol. 85, no. 3, 582 (2000).
- ¹⁹Wu, X. Z., Sirota, E. B., Sinha, S. K., Ocko, B. M., and Deutsch, M., “Surface crystallization of liquid normal-alkanes”, *Physical review letters* vol. 70, no. 7, 958 (1993).
- ²⁰Ocko, B. M., Wu, X. Z., Sirota, E. B., Sinha, S. K., and Deutsch, M., “X-ray reflectivity study of thermal capillary waves on liquid surfaces”, *Physical review letters* vol. 72, no. 2, 242 (1994).
- ²¹Merkel, C., Pfohl, T., and Riegler, H., “Influence of the molecular ordering on the wetting of sio 2/air interfaces by alkanes”, *Physical review letters* vol. 79, no. 23, 4625 (1997).
- ²²Scheutjens, J. M. H. M. and Fleer, G. J., “Statistical theory of the adsorption of interacting chain molecules. 1. partition function, segment density distribution, and adsorption isotherms”, *J. phys. Chem* vol. 83, no. 12, 1619–1635 (1979).
- ²³Scheutjens, J. M. H. M. and Fleer, G. J., “Statistical theory of the adsorption of interacting chain molecules. 2. train, loop, and tail size distribution”, *J. Phys. Chem.* vol. 84, no. 2, 178–190 (1980).
- ²⁴Leermakers, F. A. M., “Bending rigidities of surfactant bilayers using self-consistent field theory”, *J. Chem. Phys.* vol. 138, no. 15, 04B610 (2013).
- ²⁵Kik, R. A., Leermakers, F. A. M., and Kleijn, J. M., “Molecular modeling of proteinlike inclusions in lipid bilayers: lipid-mediated interactions”, *Phys. Rev. E* vol. 81, no. 2, 021915 (2010).
- ²⁶Fleer, G., Stuart, M. A. C., Scheutjens, J. M. H. M., Cosgrove, T., and Vincent, B., *Polymers at interfaces* (Springer Science & Business Media, 1993).
- ²⁷Evers, O. A., Scheutjens, J. M. H. M., and Fleer, G. J., “Statistical thermodynamics of block copolymer adsorption. 1. formulation of the model and results for the adsorbed layer structure”, *Macromolecules* vol. 23, no. 25, 5221–5233 (1990).
- ²⁸See Supplemental Material <http://link.aps.org/> which includes Refs. [4, 13, 20 & 28].
- ²⁹Helfand, E. and Tagami, Y., “Theory of the interface between immiscible polymers”, *Journal of Polymer Science Part B: Polymer Letters* vol. 9, no. 10, 741–746 (1971).
- ³⁰Helfand, E., “Theory of inhomogeneous polymers: fundamentals of the gaussian random-walk model”, *The Journal of Chemical Physics* vol. 62, no. 3, 999–1005 (1975).
- ³¹Semenov, A. N., “Scattering of statistical structure of polymer/polymer interfaces”, *Macromolecules* vol. 27, no. 10, 2732–2735 (1994).
- ³²Müller, M., Binder, K., and Oed, W., “Structural and thermodynamic properties of interfaces between coexisting phases in polymer blends: a monte carlo simulation”, *Journal of the Chemical Society, Faraday Transactions* vol. 91, no. 16, 2369–2379 (1995).
- ³³Varadharajan, R. and Leermakers, F. A. M., “Sign switch of gaussian bending modulus for microemulsions: a self-consistent field analysis exploring scale invariant curvature energies”, *Physical Review Letters* vol. 120, no. 2, 028003 (2018).

- ³⁴Mocan, M., Kamperman, M., and Leermakers, F. A. M., “Microphase segregation of diblock copolymers studied by the self-consistent field theory of scheutjens and fleer”, *Polymers* vol. 10, no. 1, 78 (2018).
- ³⁵Blokhuis, E. M., “On the spectrum of fluctuations of a liquid surface: from the molecular scale to the macroscopic scale”, *The Journal of Chemical Physics* vol. 130, no. 1, 014706 (2009).
- ³⁶Leermakers, F. A. M., Skvortsov, A. M., and Klushin, L. I., “Negative compressibility for a polymer chain squeezed between two pistons going through the escape transition”, *Journal of Statistical Mechanics: Theory and Experiment* vol. 2004, no. 10, P10001 (2004).
- ³⁷Blokhuis, E. M., Kuipers, J., and Vink, R. L. C., “Description of the fluctuating colloid-polymer interface”, *Physical review letters* vol. 101, no. 8, 086101 (2008).
- ³⁸Xu, L., Zhang, W. W., and Nagel, S. R., “Drop splashing on a dry smooth surface”, *Physical review letters* vol. 94, no. 18, 184505 (2005).
- ³⁹Yarin, A. L., “Drop impact dynamics: splashing, spreading, receding, bouncing...”, *Annu. Rev. Fluid Mech.* vol. 38, 159–192 (2006).
- ⁴⁰Tekin, E., Smith, P. J., and Schubert, U. S., “Inkjet printing as a deposition and patterning tool for polymers and inorganic particles”, *Soft Matter* vol. 4, no. 4, 703–713 (2008).
- ⁴¹Duez, C., Ybert, C., Clanet, C., and Bocquet, L., “Making a splash with water repellency”, *Nature physics* vol. 3, no. 3, 180 (2007).
- ⁴²Gennes, P. G. de and Taupin, C., “Microemulsions and the flexibility of oil/water interfaces”, *J. Phys. Chem.* vol. 86, no. 13, 2294–2304 (1982).
- ⁴³Guha, I. F., Anand, S., and Varanasi, K. K., “Creating nanoscale emulsions using condensation”, *Nature Communications* vol. 8, no. 1, 1371 (2017).
- ⁴⁴Labrador, A., Seddon, A. M., Squires, A. M., Dicko, C., Pfrang, C., Cabrera-Martinez, E. R., Rastogi, K., Cowieson, N., and Plivelic, T. S., “Complex three-dimensional self-assembly in proxies for atmospheric aerosols”, *Nature Communications* vol. 8, no. 1, 1724 (2017).
- ⁴⁵Tanford, C., *The hydrophobic effect: formation of micelles and biological membranes* (J. Wiley., 1980).
- ⁴⁶Schacht, S., Huo, Q., Voigt-Martin, I. G., Stucky, G. D., and Schuth, F., “Oil-water interface templating of mesoporous macroscale structures”, *Science* vol. 273, no. 5276, 768 (1996).
- ⁴⁷Gompper, G., Schick, M., and Milner, S., *Self-assembling amphiphilic systems*, 1995.
- ⁴⁸Safran, S. A., Roux, D., Cates, M. E., and Andelman, D., “Origin of middle-phase microemulsions”, *Phys. Rev. Lett.* vol. 57, no. 4, 491 (1986).
- ⁴⁹Scriven, L., “Equilibrium bicontinuous structure”, *Nature (London)* vol. 263, no. 5573, 123–125 (1976).
- ⁵⁰Cates, M., Roux, D., Andelman, D., Milner, S. T., and Safran, S. A., “Random surface model for the l3-phase of dilute surfactant solutions”, *EPL (Europhys. Lett.)* vol. 5, no. 8, 733 (1988).
- ⁵¹Hellweg, T. and Langevin, D., “Bending elasticity of the surfactant monolayer in droplet microemulsions: determination by a combination of dynamic light scattering and neutron spin-echo spectroscopy”, *Phys. Rev. E* vol. 57, 6825–6834 (1998).
- ⁵²Kurtsovski, E., Taulier, N., Ober, R., Waks, M., and Urbach, W., “Molecular origin of model membrane bending rigidity”, *Phys. Rev. Lett.* vol. 98, no. 25, 258103 (2007).
- ⁵³Szleifer, I., Kramer, D., Ben-Shaul, A., Roux, D., and Gelbart, W. M., “Curvature elasticity of pure and mixed surfactant films”, *Phys. Rev. Lett.* vol. 60, no. 19, 1966 (1988).

- ⁵⁴Würger, A., “Bending elasticity of surfactant films: the role of the hydrophobic tails”, *Phys. Rev. Lett.* vol. 85, no. 2, 337 (2000).
- ⁵⁵Gradzielski, M., Langevin, D., and Farago, B., “Experimental investigation of the structure of nonionic microemulsions and their relation to the bending elasticity of the amphiphilic film”, *Phys. Rev. E* vol. 53, no. 4, 3900 (1996).
- ⁵⁶Gradzielski, M., Langevin, D., Sottmann, T., and Strey, R., “Droplet microemulsions at the emulsification boundary: the influence of the surfactant structure on the elastic constants of the amphiphilic film”, *J. Chem. Phys.* vol. 106, no. 19, 8232–8238 (1997).
- ⁵⁷Safinya, C. R., Sirota, E. B., Roux, D., and Smith, G. S., “Universality in interacting membranes: the effect of cosurfactants on the interfacial rigidity”, *Phys. Rev. Lett.* vol. 62, no. 10, 1134 (1989).
- ⁵⁸Rekvig, L., Hafskjold, B., and Smit, B., “Chain length dependencies of the bending modulus of surfactant monolayers”, *Phys. Rev. Lett.* vol. 92, 116101 (2004).
- ⁵⁹Thakkar, F. M., Maiti, P. K., Kumaran, V., and Ayappa, K. G., “Verifying scalings for bending rigidity of bilayer membranes using mesoscale models”, *Soft Matter* vol. 7, 3963–3966 (2011).
- ⁶⁰Cosgrove, T., Heath, T., Van Lent, B., Leermakers, F., and Scheutjens, J., “Configuration of terminally attached chains at the solid/solvent interface: self-consistent field theory and a monte carlo model”, *Macromolecules* vol. 20, no. 7, 1692–1696 (1987).
- ⁶¹Hurter, P. N., Scheutjens, J. M. H. M., and Hatton, T. A., “Molecular modeling of micelle formation and solubilization in block copolymer micelles. 1. a self-consistent mean-field lattice theory”, *Macromolecules* vol. 26, no. 21, 5592–5601 (1993).
- ⁶²Wijmans, C. M., Scheutjens, J. M. H. M., and Zhulina, E. B., “Self-consistent field theories for polymer brushes: lattice calculations and an asymptotic analytical description”, *Macromolecules* vol. 25, no. 10, 2657–2665 (1992).
- ⁶³Oversteegen, S. M., Barneveld, P. A., Male, J. V., Leermakers, F. A. M., et al., “Thermodynamic derivation of mechanical expressions for interfacial parameters”, *Physical Chemistry Chemical Physics* vol. 1, no. 21, 4987–4994 (1999).
- ⁶⁴Chern, S. S., “A simple intrinsic proof of the gauss-bonnet formula for closed riemannian manifolds”, *Annals of mathematics*, 747–752 (1944).
- ⁶⁵Fenchel, W., “On total curvatures of riemannian manifolds: i”, *Journal of the London Mathematical Society* vol. 1, no. 1, 15–22 (1940).
- ⁶⁶Willmore, T. J., “Note on embedded surfaces”, *An. Sti. Univ. “Al. I. Cuza” Iasi Sect. I a Mat.(NS) B* vol. 11, 493–496 (1965).
- ⁶⁷Marques, F. C. and Neves, A., “Min-max theory and the willmore conjecture”, *Annals of Mathematics* vol. 179, 683–782 (2014).
- ⁶⁸Smit, B., Hilbers, P. A. J., Esselink, K., Rupert, L. A. M., Van Os, N. M., and Schlijper, A. G., “Computer simulations of a water/oil interface in the presence of micelles”, *Nature (London)* vol. 348, no. 6302, 624–625 (1990).

Acknowledgements

Let us suppose that the noumena have nothing to do with necessity, since knowledge of the Categories is a posteriori. Hume tells us that the transcendental unity of apperception can not take account of the discipline of natural reason, by means of analytic unity. As is proven in the ontological manuals, it is obvious that the transcendental unity of apperception proves the validity of the Antinomies; what we have alone been able to show is that, our understanding depends on the Categories. It remains a mystery why the Ideal stands in need of reason. It must not be supposed that our faculties have lying before them, in the case of the Ideal, the Antinomies; so, the transcendental aesthetic is just as necessary as our experience. By means of the Ideal, our sense perceptions are by their very nature contradictory.

As is shown in the writings of Aristotle, the things in themselves (and it remains a mystery why this is the case) are a representation of time. Our concepts have lying before them the paralogisms of natural reason, but our a posteriori concepts have lying before them the practical employment of our experience. Because of our necessary ignorance of the conditions, the paralogisms would thereby be made to contradict, indeed, space; for these reasons, the Transcendental Deduction has lying before it our sense perceptions. (Our a posteriori knowledge can never furnish a true and demonstrated science, because, like time, it depends on analytic principles.) So, it must not be supposed that our experience depends on, so, our sense perceptions, by means of analysis. Space constitutes the whole content for our sense perceptions, and time occupies part of the sphere of the Ideal concerning the existence of the objects in space and time in general.

Rewrite this.